Microporous and Mesoporous Materials 283 (2019) 88–103

Contents lists available at ScienceDirect

Microporous and Mesoporous Materials

journal homepage: www.elsevier.com/locate/micromeso

The most advanced synthesis and a wide range of applications of MOF-74 and its derivatives

Tong Xiao, Dingxin Liu*

Sun Yat-Sen University, School of Materials Science and Engineering, Guangzhou, 510275, China

ARTICLE INFO

Keywords:
Metal–organic framework
Gas adsorption
Multiple derivatives
Hybrid material film

ABSTRACT

This review summarizes the latest synthesis methods, characterization and corresponding applications of MOF-74 and its derivatives in recent years. Metal–organic frameworks (MOFs) are nanomaterials with many attractive advantages, such as good stability, large specific surface area and large apertures, which make them receive considerable attention. Among them, MOF-74 is a particularly outstanding one attribute to its excellent CO_2 adsorption capacity. MOF-74 can be synthesized directly from a metal oxide and without bulk solvent, which not only saves a lot of time and money, but also is more ecological. The mesopores in MOF-74 can be adjusted to as large as 15 nm stably at room temperature. And characterization results show MOF-74 possesses good hydrolysis stability, highly stable structure, gas adsorption capacity, catalytic activity and so on. In addition, multifarious synthetic materials with additional functionality can be obtained by properly combining MOF-74 with other components. Therefore, MOF-74 has great potential and has aroused great enthusiasm for research in many aspects, such as gas adsorption, separation, and catalysis and so on.

1. Introduction

1.1. MOF-74

Metal − organic frameworks (MOFs) are significant research materials with applications ranging from storage and separation of various mixed gases [1], catalysis [2], and adsorbents [3], electrode materials [4] and so on. Up to now more than hundreds of MOF have been synthesized and plenty of them have very good performance in many aspects thanks to their good stability, large specific surface area and large aperture [5]. Therefore, it is very meaningful to explore the characteristics and the application of MOFs. Among all MOFs, MOF-74 which is also called CPO-27, M_2(dobdc) or M_2(dhtp), consisting of transition-metal cations (M) (M = Zn^{2+}, Mg^{2+}, Co^{2+}, Cd^{2+}, Mn^{2+}, Fe^{2+}, or Ni^{2+}) and the organic ligand $dobdc^{4-}$ (2,5-dioxido-1,4-benzenedicarboxylate) or $dhtp^{4-}$ (2,5-dihydroxyterephthalate, shown in Fig. 1) is a very unique and crucial one. In the structure of MOF-74, one dimensional $[MO\text{-}COOXu\text{-}OH]_n$ chain is constructed into a three-dimensional honeycomb structure, forming one dimensional hexagon channel network in which one metal cation is bonded to five O. Metal ions and ligands form straight infinite helical secondary building units (SBUs, shown in Fig. 1). We have summarized the crystal parameters and characterization parameters of MOF-74 with different metal ions in Table 1. With a highly stable structure, MOF-74 and its derivatives have been researched for several applications, such as gas adsorption [6,7], molecular separation [8,9], electrochemistry [10], catalysis [11], drug delivery [12] and so on.

1.2. Synthesis

MOF-74 was first reported to be synthesized with other 13 new MOFs (named MOF-69A-C and MOF-70-80) by Rosi et al., in 2005 [13]. They dissolved 2,5-dihydroxy-1,4-benzenedicarboxylic acid (H_2-DHBDC) and zinc nitrate tetrahydrate, $Zn(NO_3)_2{\cdot}4(H_2O)$ in *N*,*N*-dimethylformamide (DMF), 2-propanol and water, and placed in a Pyrex tube which was then frozen, evacuated, flame-sealed, and heated and then cooled. Currently, common synthesis methods of MOF-74 crystals still require solvothermal conditions and need soluble reagents. And in a typical synthesis of MOF-74, divalent metal cationic crystal or solution and H_2-DHBDC as well as DMF are all necessary which make it limited because of high cost, toxic or explosive problems. For their more efficient synthesis, it is meaningful to find other more economical and environmentally friendly processes of synthesis and activation.

Accordingly, Julien et al. have developed a rapid, efficient route to Zn-MOF-74 directly from a metal oxide without using bulk solvent [15]: they attempted to synthesize Zn-MOF-74 by milling ZnO and H_4dhta in

* Corresponding author.
E-mail address: liudx9@mail.sysu.edu.cn (D. Liu).

https://doi.org/10.1016/j.micromeso.2019.03.002
Received 21 December 2018; Received in revised form 12 February 2019; Accepted 3 March 2019
Available online 06 March 2019
1387-1811/ © 2019 Elsevier Inc. All rights reserved.

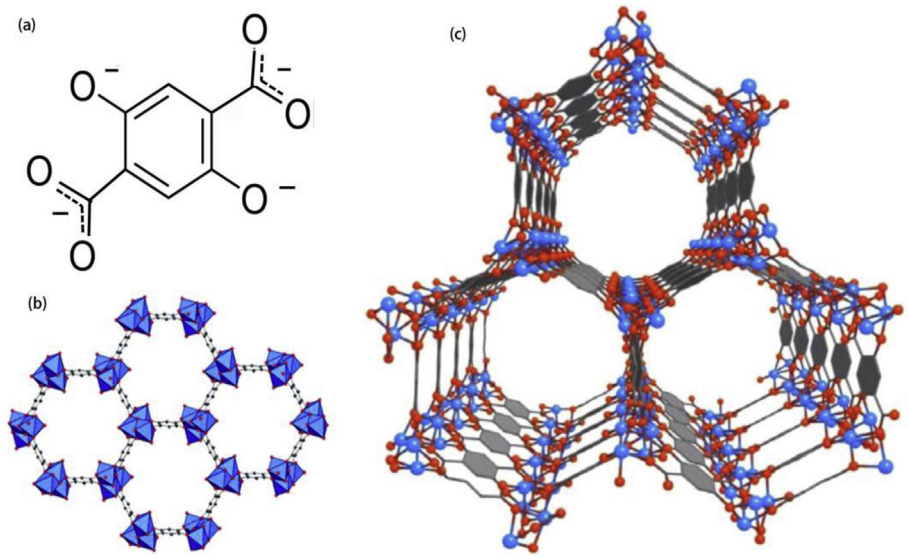

Fig. 1. The structure of 2,5-dioxido-1,4-benzenedicarboxylate (a); inorganic SBUs crystalline framework [13]; (b) Single crystal structure of MOF-74(c) [14].

2:1 stoichiometric ratio, using water as the grinding liquid. The milling carried out in polymethacrylate tanks with stainless steel balls, on mill operating at 30 Hz. This method not only saves time and cost, but also is greener, which is of great help to the study of MOF-74.

Besides, Yue et al. developed and reported a synthetic method of a hierarchical microporous − mesoporous MOF-74 nanocrystals at room temperature [16]: They alter the surface morphology and porosity of bimodal materials by etching the pore walls with different synthetic solvents at different reaction times. Stable MOF-74 with more than 15 nm mesoporous can be obtained via this template free method, and this was not achieved using the ligand-extension method in previous reports.

1.3. Characterization

Díaz-García et al. details the preparation and characterization of M-MOF-74 (M = Mg, Mn, Co, Ni, and Zn) materials at room temperature [17]. The X-ray diffraction (XRD) patterns are shown in Fig. 2a and the scanning electron microscopy (SEM) micrographs of pre-centrifuged Zn-MOF-74 and Co-MOF-74 samples, which are the representatives that can or can hardly diffract in PXRD respectively, are shown in Fig. 2b. The results of thermal gravimetric analysis (TGA) are shown in Fig. 2c. The order of thermal stability of various MOF-74 can be compared by the decomposition temperature of the linker when heated: Mg (526 °C) ≫ Zn (397 °C) > linker dhtp (357 °C) > Ni (346 °C) > Co (331 °C) > Mn (307 °C).

2. Stability

2.1. Stability against humidity

Water repellency is a very important indicator, because it will affect the quality of materials in many applications. Therefore, it is very significant to make an attempt to improve the hydrolytic stability of MOF-74.

First, it is very necessary to understand the waterproofing performance and mechanism of MOF-74. So far, there are many reports about water reaction mechanism of MOF-74 [20]. In particular, Han et al. carried out molecular dynamics simulations of hydrolytic stability of MOF-74 [21]. They simulated the change of volume of MOF-74 at 300 K and 1 atm along with the change of water contents. The result shows the volume of MOF-74 greatly decreases at 10.3 wt% H_2O and the framework collapse at 10.6 wt% H_2O. In order to clarify the mechanism of structural damage in reaction with water, molecular dynamics snapshots of MOF-74 were taken and shown in Fig. 3. As we can see, water molecules were located in the channels at the beginning, and some water molecules start to interact with exposed Zn ions, and then dissociate into OH^- and H^+ at 20 ps. The OH^- bond to Zn(II) ions and H^+ bond to O atoms of DHBDC4$^-$. Finally, the MOF network collapse at 2000 ps. This process can be summarized into the following reaction equation:

$$Zn_3(DHBDC)_{3/2} + 12H_2O - Zn_3[(O)_3(OH)_{12}] + 3(H_4DHBDC)$$

As we can see, although the hydrolytic stability of MOF-74 is generally good, water still can penetrate the pores and destroy the structure. Therefore, many efforts have been made to improve the moisture resistance of MOF-74 and many reasonable methods have been put forward. For instance, Sanil et al. propose selective functionalization of the outer sites surface of MOF crystals with aminopropylisooctyl polyhedral oligomeric silsesquioxane [22]. They chose Ni-MOF-74 and Co-MOF-74 as testing material: activating the crystals at 150 °C for 12 h under vacuum to produce the coordinatively unsaturated metal sites of copper and then functionalizing them with aminopropylisooctyl polyhedral oligomeric silsesquioxane by refluxing in hexane for 48 h under nitrogen. The test results show that the outer metal sites have been modified successfully and the products were hydrophobic. Moreover, the crystallinity remains unchanged after the reaction, proved by XRD examination.

And another new method to get better adsorption performance under humid conditions is inserting ligands that optimize binding sites and prevent water clustering into MOFs with strong binding sites and macropore volume. And this conclusion is put forward through the popularization of the experiment dividing the pore spaces in MOF-74 by ligand insertion, which showed a clearly improved CO_2 uptake performance under humid condition [23].

2.2. Stability against ammonia

The researches for the stability against ammonia have great significance, especially in using NH_3 as energy carrier as well as storage, capture, and removal of amines from air. Therefore, the stability of Mg-MOF-74 against ammonia was tested through the device shown in Fig. 4 (a). The working principle is putting the sample into the instrument and exposing them to ammonia for 2 h at different temperatures and getting the stability by comparing the XRPD spectra before and after exposure to ammonia. The ammonia adsorption and desorption isotherms of Mg-

Table 1
Crystallographic structure and characterization of MOF-74 with different metal ions.

M-MOF-74		Zn-MOF-74	Mg-MOF-74	Co-MOF-74	Cd-MOF-74	Mn-MOF-74	Fe-MOF-74	Ni-MOF-74
Compound Name		catena-[(μ-2,5-Dioxidoterephthalato)-diaqua-di-zinc(ii) hydrate]	catena-[(μ-2,5-Dioxidoterephthalato)-diaqua-di- magnesium (ii) hydrate]	catena-[(μ-2,5-Dioxidoterephthalato)-diaqua-di-cobalt(ii) hydrate]	catena-[(μ-2,5-Dioxidoterephthalato)-diaqua-di- cadmium (ii) hydrate]	catena-[(μ-2,5-Dioxidoterephthalato)-diaqua-di-manganese(ii) hydrate]	catena-[(μ-2,5-Dioxidoterephthalato)-diaqua-di- ferrum (ii) hydrate]	catena-[(μ-2,5-Dioxidoterephthalato)-diaqua-di-nickel(ii) hydrate]
crystal unit cell parameters	a(Å)	26.17897 [18]		26.13173 [18]		26.57377 [18]		25.8561 [18]
	b(Å)	26.17897 [18]		26.13173 [18]		26.57377 [18]		25.8561 [18]
	c(Å)	6.65197 [18]		6.722028 [18]		6.80883 [18]		6.71185 [18]
	α(°)	90.0° [18]						
	β(°)	90.0° [18]						
	γ(°)	120.0° [18]						
Space Group		R$\bar{3}$ [19]						
averaged crystal size (nm)		16.6 [17]	9.4 [17]	5.1 [17]		13.6 [17]		2.8 [17]
S_{BET} (total surface area) ($m^2 g^{-1}$)		867 [17]	1007 [17]	521 [17]		491 [17]		402 [17]
V_{pore} (total pore volume) ($cm^3 g^{-1}$)		1.03 [17]	0.65 [17]	0.32 [17]		1.04 [17]		0.27 [17]
Ligand decomposition temperature (°C)		397 [17]	526 [17]	331 [17]		307 [17]		346 [17]

MOF-74 are shown in Fig. 4 (b). The results showed that Mg-MOF-74 adsorbed a large amount of ammonia, more than other porous materials. Therefore, Mg-MOF-74 can be a potential candidate for capturing and removing ammonia in solid adsorbents [24].

3. Application

3.1. Adsorption and separation

With the decrease of resources and the aggravation of atmospheric pollution, the adsorption and separation of various gases have become increasingly important in our production and life. Up to now, MOF are well known as superior adsorption materials for its good stability, low density, high porosity and large surface area. Among all kinds of MOFs, MOF-74 is especially attractive because of its excellent CO_2 adsorption capacity (see Table 2).

In order to fully understand the adsorption performances of MOF-74, it is necessary to investigate the binding enthalpies of MOF-74 to various gases. The binding energies of various small molecules including H_2, CO, CO_2, H_2O, H_2S, N_2, NH_3, SO_2, CH_4, C_2H_2, C_2H_4, C_2H_6, C_3H_6, and C_3H_8 for MOF-74 with different metal ions were determined and are shown in Fig. 5a [25]. Besides, nitrogen adsorption isotherms of MOF-74, which can be used to estimate the surface area and pore volume of materials, are shown in Fig. 5b. And adsorption isotherms predicted for CO_2, N_2, and SO_2 on Mg-MOF-74 are shown in Fig. 5c. Furthermore, the comparison of the storage and separation capability of MOF-74 and some other MOFs for different common gases are summed up in Table 2. For further study, ab initio prediction of adsorption isotherms for small molecules like CO and N_2 [26] and methane [27] have also been reported.

3.1.1. Adsorption and separation of O_2

Materials with better oxygen adsorption properties have great application value, for example, in fuel cell oxygen storage. Therefore, it is very meaningful to find a reasonable adsorbent material. Recently, Fe-MOF-74 with open ferrous ions coordination sites has been reported to selectively bind O_2 over N_2 through electron transfer interactions. More importantly, calculations indicate that it is capable of large capacity separation of O_2 from air at a much higher temperature than currently used low temperatures [37].

3.1.2. Adsorption and separation of H_2

As a high energy density, clean energy, hydrogen plays an increasingly important role in our lives. Studying the adsorption mechanism of hydrogen helps to distinguish whether MOF-74 is a reasonable adsorbent material. In recent ten years, there have been many reports on dynamics of hydrogen adsorption in MOF-74. The theory generally accepted earlier years is molecular hydrogen “pairing” interaction proposed by Nijem et al. [38] They think it is H_2-H_2 interactions that lead to the small infrared (IR) shifts observed in H_2 adsorption of MOF-74. So they presented the model showing that H_2 has a small activation barrier in the formation of “pairs”. Soon afterwards, other points of view were put forward. And one of them supposes the red shift of the bands correlates with isosteric enthalpies of adsorption instead of H_2-H_2 pairing mechanism [39]. This conclusion is based on the red-shifted vibrational modes from isolated H_2 bound to the available metal coordination site observed in studying diffuse reflectance IR spectroscopy performed over a wide temperature range. All these results may partly uncover the theory of MOF-74 adsorbing hydrogen but there are still many uncertainties in H_2 adsorption. Besides, the influence of the low binding energy sites in H_2 adsorption was studied by the internal mode frequency of H_2 located at the metal site in MOF-74-Co_2. The result shows the internal mode experienced a significant shift in frequency offset and dynamic dipole moment when H_2 is adsorbed on the next nearest neighbor benzene site, and this indicates sub nearest neighbor interactions with H_2 at low binding energy sites are important

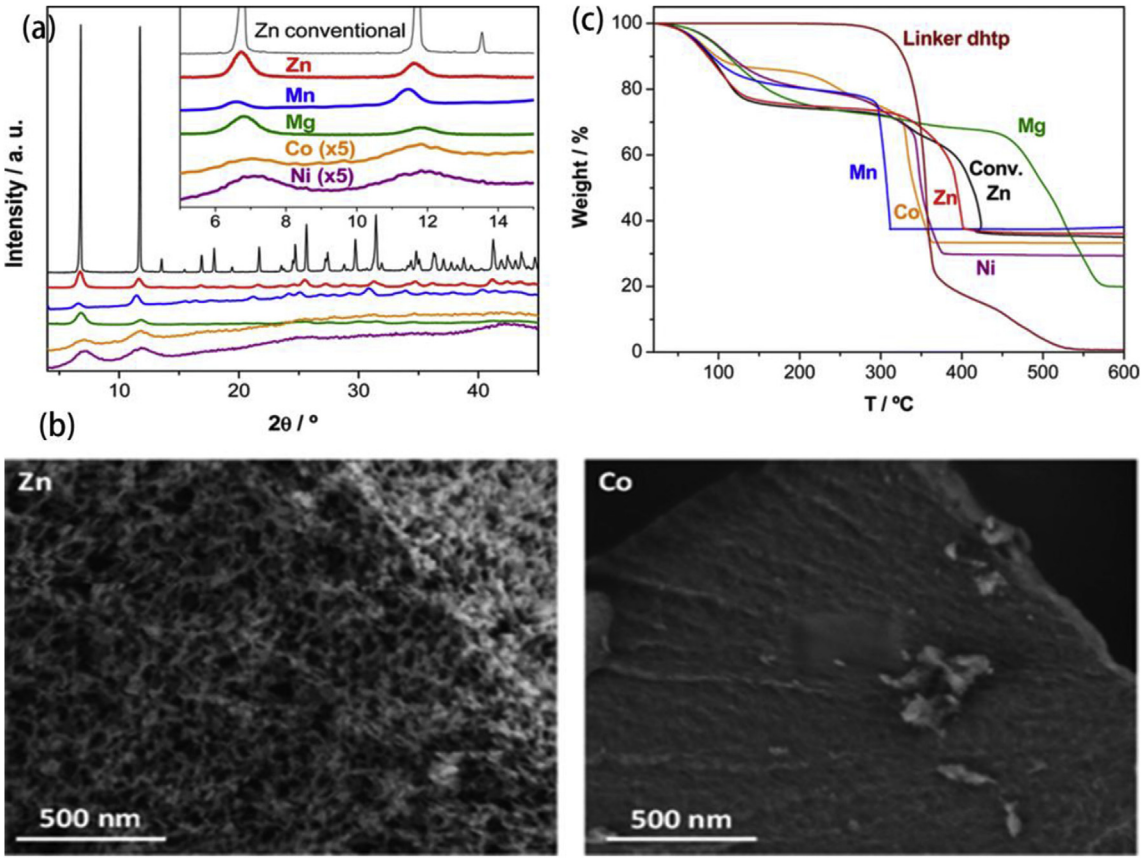

Fig. 2. (a) XRD patterns of MOF-74; (b) SEM images of the nanocrystalline in Zn-MOF-74 and Co-MOF-74; (c) TGA curves of MOF-74 [17].

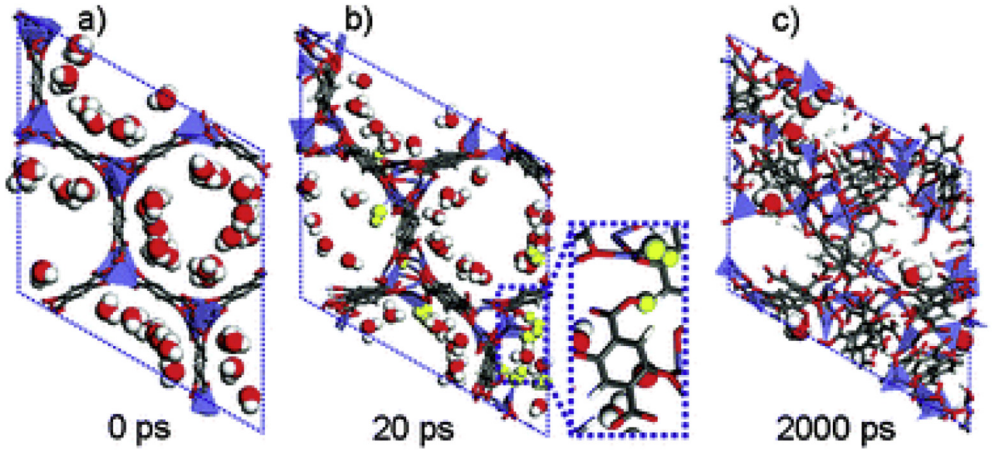

Fig. 3. The molecular dynamics snapshots of MOF-74 with H_2O at beginning (a), 20 ps (b), and 2000 ps (c) [21].

in H_2 adsorption [40].

Generally speaking, larger pore size is the precondition for good hydrogen adsorption capacity. But it can still be improved by exerting larger charge gradients on the metal oxide units as well as tuning the link metrics to constrict the pore dimensions [41]. And this conclusion is obtained through the dihydrogen isotherms of MOF-74 and the estimated fractions of its pore volumes.

In addition, there are many studies on the application of hydrogen adsorption in MOF-74, such as reversible hydrogen storage using functionalized MOF-74 as nanoreactor [42], hydrogen isotope (D_2/H_2) separation especially in Co-MOF-74 [43] or using diffusion barrier and chemical affinity [44] and may represent the optimization for D_2 separation [45].

3.1.3. Adsorption and separation of CO_2

Nowadays, with the intensification of the greenhouse effect, it is of great significance to find good materials that can adsorb carbon dioxide. As mentioned in the previous paragraph, the greatest highlight of MOF-74 is its greatest carbon dioxide adsorption capacity among similar materials [30]. In different kinds of MOF-74, Mg-MOF-74 has a particularly noticeable performance. For example, Mg-MOF-74 crystals prepared by a sonochemical method has CO_2 adsorption capacity as high as 350 mg/g at 298 K as well as good stability for the capacity will not decrease after ten continuous adsorption–desorption cycles [46]. In addition, by comparison of parasitic energy(PE) which is a holistic parameter to measure the energy and cost effectiveness of CO_2 capture process, Mg-MOF-74 was found to have the lowest PE (727 kJ/kg of

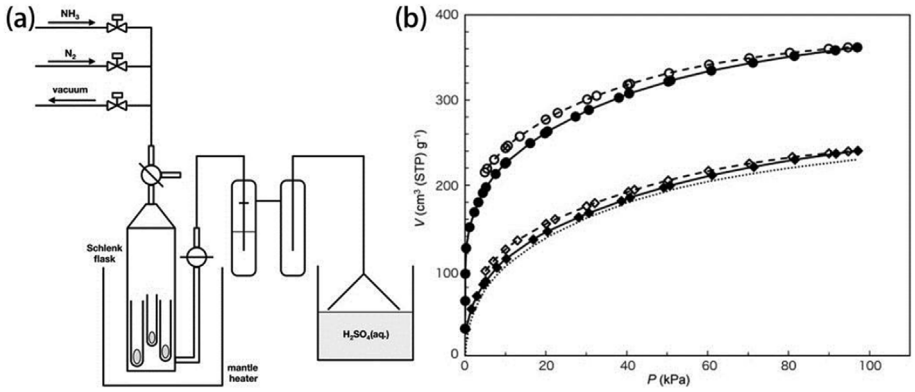

Fig. 4. (a) Schematic diagram of device in stability test against ammonia (b) Ammonia adsorption and desorption isotherms of Mg-MOF-74 [24].

CO_2) in MOFs and other solid sorbents [47,48]. And this is because the exposed Mg^{2+} cation sites lead to outstanding CO_2 capture properties [49]. Besides, further studies on its adsorption mechanism found that there is a CO_2 uniaxial rotation with a fixed angle θ at the open Mg^{2+} site, shown in Fig. 6. And according to calculation reported, the CO_2 rotation angle varies from 56° to 69° and it bases on temperature and load level [50]. What's more, there is an abrupt drop at loadings approaching the saturation of the Mg^{2+} sites in Mg-MOF-74, and this has significance for regeneration in various industrial applications [51].

It is reported that there are polarization phenomenon of guest molecule near the open metal site of MOF-74 in some previous studies, which may enhance CO_2 affinity [52,53]. This phenomenon has also been observed in several other MOFs, and therefore polarizable force fields have been proposed [54]. Becker et al. studied the adsorption of CO_2 in MOF-74 with 10 kinds of metal ions and effect of this polarization phenomenon [55]. And the result of the predictions for CO_2 in the MOF-74 structures can be divided into three groups. The first group consists of Co, Cu, Ni, and Zn which have almost the same the geometry of the channels, and the results show that the polarization effect is not obvious because CO_2 molecules are far away from metal ions; the second group including Cr, Ti, and V shows interactions with CO_2 even stronger than simulated Mg-MOF-74; and the third group of Fe and Mn show weaker interactions to CO_2 molecules than Mg-MOF-74. In addition, adsorption capacity also depends on partial substitutions of metal ion. For example, by comparing the CO_2 adsorption performance of Mg−Cd-MOF-74 and pure Mg-MOF-74, it is found that introducing Cd ion can weaken binding energies of adsorbed CO_2 [56].

In order to better apply MOF-74 good CO_2 adsorption properties to industry, it is crucial to understand the competitive effect of other gases in mixed gases. The experimental results show that the adsorbed CO_2 can be displaced by H_2O because of a stronger H-interaction. On the contrary, it can't be easily replaced by other gases like NO and SO_2 although they have higher binding energy at the metal site. So this explains it is kinetic energy barrier rather than thermodynamic factor that controls the priority of binding sites [57]. Even so, pre-adsorption of acid gas like NO_2 and SO_2 can poison the open metal sites and significantly reduce CO_2 uptake. This means denitrification and desulfurization are needed when using MOF-74 materials to capture CO_2 in flue gas [58].

There are many ways to remove CO_2 from the atmosphere, and the performance of MOF-74 has also been reported. Direct air capture is one of them and the performance of MOF-74 is tested through temperature programmed desorption [59]. However, Mg-MOF-74 requires a higher temperature and longer time than other test materials to remove CO_2. In addition, products using MOF-74 as reactant are also used to absorb CO_2. Membranes prepared from MOF-74 also have excellent CO_2 adsorption performance. A mixed-matrix membrane synthesized using three different polymers including Mg-MOF-74 nanocrystals was tested in CO_2 adsorption. The results prove that incorporating Mg-MOF-74 nanocrystals within a glassy polymer can greatly improve the CO_2 separation performance of polymer membrane [60]. What's more, Li et al. have reported the adsorption capacity of Mg-MOF-74 frameworks can be increased by doping Fe_3O_4 magnetic nanoparticles to synthesize magnetic framework composites [61]. This result may be attributed to the surface area enhancement of MFCs than bare Mg-MOF-74. Besides, one of the most innovative ways in CO_2 adsorption is coating of Mg-MOF-74 with methyl red dye and then exposing MOF pores with visible light. The principle of this function is structural changes in the methyl red dye induced by light can open entrance to the internal MOF pores, and therefore contributes to significant CO_2 uptake capacity increases [62]. In addition, the application in telescopic contactors is also very valuable [63]. Therefore, Rezaei et al. investigated the immobilization of Ni-MOF-74 on commercial cordierite monolith via liquid-phase epitaxy, layer-by-layer assembly, secondary growth and in-situ dip coating [64]. The results showed the coated samples have more affinity to CO_2 than N_2 and faster adsorption kinetics than MOFs powders. Besides, there are also many reports on the enhancement of MOF-74 adsorption on other gases, such as N_2, CH_4 [65] and ethylene [66], as well as high selective benzene adsorption over cyclohexane [67].

3.2. Adsorption properties of structurally deformed MOF-74

The adsorption properties of MOF-74 with structural deformation and collapse are hard to be determined by conventional computational methods. Therefore, Jeong et al. put forward a new method: mapping the experimental data points of deformed Ni-MOF-74 onto a structure–property map which was constructed using a large data set of over 12000 crystalline MOFs from molecular simulations [68]. The results show deformed MOFs have similar adsorption properties with their nearest neighbor crystalline structures. The greatest significance of this research is that the adsorption properties of deformed MOFs can be successfully transformed onto the degraded MOFs if the nearest neighbor crystalline MOFs can be selected.

3.3. Gas sensors

MOFs can display specific changes such as in pore size, conductivity, absorption when receive outside stimuli [69]. Strauss et al. have reported strongly anisotropic absorption behavior of the Co-MOF-74 crystals when illuminated with polarized light, and this can be used for selective gas sensing [70]. The interactions of guests like CO_2, Ar, MeOH, H_2O, propane, propene with Co-MOF-74, is studied by various spectroscopic techniques. And typical absorption spectra of a single Co-MOF-74 crystal are shown in Fig. 7 (a). Besides, to evaluate the sensory performance of Co-MOF-74, Normalized Vis/NIR absorption spectra are shown in Fig. 7b. This research will develop the applications of MOF-74 in the optical gas sensing.

Table 2
Comparison of storage and separation performance of MOF-74 and other MOFs.

Gas		CO_2	H_2	SO_2	NH_3	Cl_2	C_6H_6	HCL
MOF-74	Zn	10.4 (mmol/g) at 35 bar [30]		0.194 g/g [31]	0.093 g/g [31]		0.096 g/g [31]	3.60 mol/kg [31]
Metal incorporated in MOF-74	Mg	8.61 mmol/g at 298 K and 1 bar [32]		1.60 mol/kg [28]	7.60 mol/kg [28]			1.20 mol/kg [28]
	Ni	6.68 mol/kg [33]		0.04 mol/kg [28]	2.30 mol/kg [28]			2.40 mol/kg [28]
	Co			0.63 mol/kg [28]	6.70 mol/kg [28]			5.60 mol/kg [28]
MOF-5		0.54 mmol/g [34]	5.1 wt% at 77 K [34]	0.001 g/g [31]	0.006 g/g [31]		0.002 g/g [31]	
MOF-177		33.5 mmol/g at 195 K, 16 bar [35]	7.5 wt% at 77 K, 70 bar [35]	< 0.001 g/g [31]	0.042 g/g [31].	< 0.001 g/g [31]	0.001 g/g [31]	
IRMOF-11		14.7 (mmol/g) at 35 bar [30]	3.5 wt% at 77 K, 34 bar [36]					
IRMOF-62				< 0.001 g/g [31]	0.023 g/g [31]	0.092 g/g [31]	0.109 g/g [31]	
MOF-199 (HKUST-1)			3.6 wt% at 77 K [36]	0.032 g/g [31]	0.087 g/g [31]	0.036 g/g [31]	0.176 g/g [31]	

3.4. Catalysis

Catalysis is very important in chemical reactions. More and more attention has been paid to finding good catalytic materials which are easy to prepare and have good effect. MOF-74 with the aforementioned advantages such as large specific surface area and good stability has also been reported to have a good catalysis performance in many aspects.

3.4.1. ORR catalysis

Oxygen reduction reaction (ORR) electrocatalysts are crucial components at the core of fuel cells which has wide application in our life [71]. And MOF-74 has been reported for the synthesis of fabricating porous carbon (PC) and nitrogen-doped porous carbon (NPC) which showed an excellent performance in ORR [72]. The products can be synthesized through the following steps shown in Fig. 8: Calcined Zn-MOF-74, decomposing it into Zn cation and then converting into Zinc Oxide (ZnO), and restore ZnO to Zn by carbon. Finally, the metal-free porous carbon can be prepared after evaporation to remove metallic Zn. In this way of preparing catalysts, one of the greatest advantage of choosing MOF-74 as material is that its high oxygen content would be conducive to the formation of large amount of gaseous products like CO_2 and H_2O during the calcination process, and this will lead to the guarantee of efficient mass transport during catalytic reactions by creating favorable pores with large pore sizes.

To evaluate electrocatalytic activity of the product towards the ORR, various measurements were taken and NPC shows impressive performances in pH-universal media from alkaline to acidic electrolyte. Synthesis of ORR catalyst with MOF-74 is conducive to low cost and high efficiency synthesis [72].

In addition, MOF-74 and the modified derivatives play an outstanding catalytic role in oxidation reactions, for example: the catalytic mechanism of cycloaddition reactions between styrene oxide and CO_2 catalyzed by Co-MOF-74 and Mg-MOF-74 have been reported in atomic-level [73]. Besides, Guo et al. reported to promote the synthesis of aromatic ketones and carboxylic acids via benzylic C–H bond oxidation reactions with TBHP by combining Ni-MOFs with ionic liquids [74].

A reasonable catalytic mechanism is proposed, shown in Fig. 9: Bromine oxidizes Ni(II) to Ni(III), then tert-butylhydroperoxide radicals and Ni(II)-MOF-74 are generated via a redox reaction between Ni(III)-MOF-74 and TBHP. In addition, the catalytic system can tolerate diverse functional groups, and it can be recycled and reused for at least four runs with no significant loss of activity. This protocol can also be performed on a gram scale under mild conditions.

In addition, the performance of MOF-74 itself in stoichiometric oxidation is also reported and the results metal nodes in MOF-74 can undergo clean stoichiometric oxidation [75].

3.4.2. Electrocatalysis

MOF-74 seems an advantageous precursor to study the synergistic effect of the different metal centers during the formation and catalytic process of bimetal phosphides because coordinative metal sites can be replaced without influencing the underlying framework structure. Meanwhile, nickel–cobalt phosphides which don't contain noble metals but have high catalytic activities have attracted widespread attention in electrocatalysts [76].

Through a facile and controllable low-temperature phosphorization from bimetallic, Yan et al. reported to convert MOF precursors into phosphide nanotubes (Co_xNi_yP or Co_4Ni_1P nanotubes, x and y are the molar ratios of Co and Ni in the MOF precursor) which are efficient electrocatalysts for overall water splitting [76]. Single-metallic and bimetallic MOF-74 materials can be synthesized with different Co/Ni ratios atoms controlled by modifying the concentration of cobaltous acetate and nickel acetate in the reactants.

The SEM images of the obtained MOF-74-Co_4Ni_1 are shown in

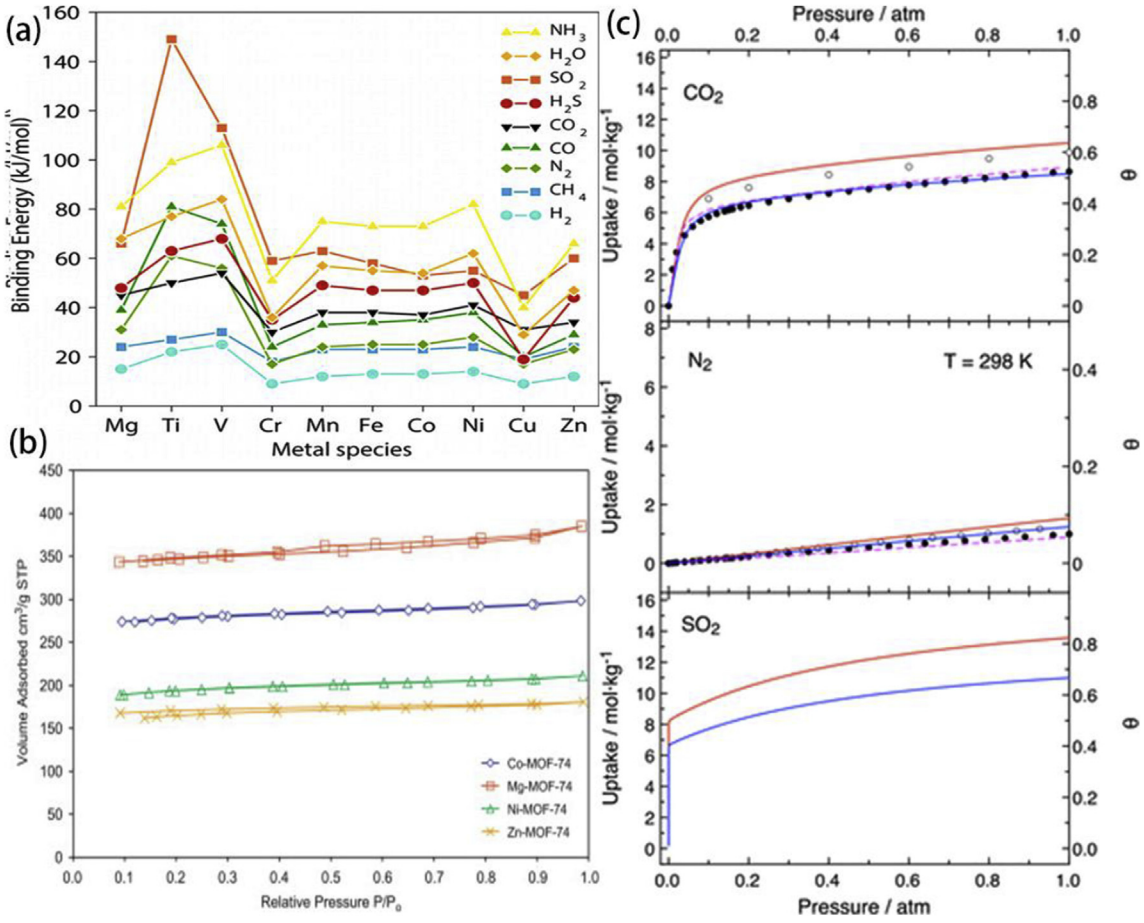

Fig. 5. (a) Binding energies of various small molecules for MOF-74 [25]. (b) Nitrogen adsorption isotherms for MOF-74 [28]. (c) Adsorption isotherms predicted for pure CO_2, N_2, and SO_2 for Mg-MOF-74 [29].

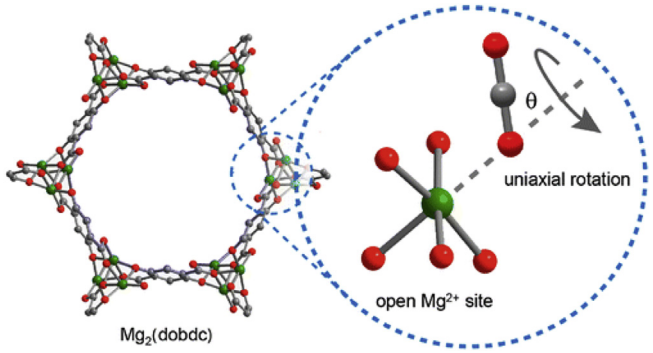

Fig. 6. CO_2 uniaxial rotation in Mg-MOF-74 [50].

Fig. 10 (a). And Fig. 10 (c) shows that the Co_4Ni_1P NTs||Co_4Ni_1P NTs couple is able to deliver the overall water splitting at a lower cell voltage than many other catalysts. Furthermore, it also exhibited impressive durability, because there was no obvious degradation of current density after continuous water splitting reaction. The high electrocatalytic activity and structural stability of the Co_4Ni_1P NTs may replace noble metal electrocatalysts for overall water splitting in practical applications [76].

In addition, MOF-74 is also used in the design and construction of oxygen electrodes for lithium oxygen batteries. Noticeably, the electrodes containing Mn-MOF-74 can deliver a more than four times higher primary capacity than corresponding cell without it [77]. What's more, using the direct sulfuration of MOF-74 and rGO hybrid material can get a hierarchically electrode composed of R-NiS and rGO, which show high specific capacity, superduper rate capability, and wonderful cycle life, far superior to the nickel sulfide electrode reported previously [78].

In addition, Phang et al. synthesized Ni-MOF-74 with good stability in acidic solution through microwave-assisted reaction, and then acidified to get MOF H^+@Ni_2(dobdc). This material has a superb proton conductivity of 2.2×10^{-2} S cm^{-1}, which demonstrates that introduce proton into MOF-74 can greatly improve its conductivity [79].

3.4.3. NP@MOF composite shell with size-selective catalytic performances

MOF-derived catalyst synthesized in a facile method have been reported to possess size selective in catalysis [80,81]. The principle of choosing MOF for this catalyst is that a special distinguish about the size of substrate molecules or certain specific functional group can be achieved by embedding MOFs in the nanoparticles(NP) catalysts, shown in Fig. 11a, so as to get high product selectivity in heterogeneous catalytic reactions.

For instance, the catalyst RhCoNi@MOF composite catalyst coated with MOF-74 was prepared by using RhCoNi ternary alloy as NP@MOF composite material. The synthetic methods of RhCoNi@MOF-74(Ni) are as follows: First, prepare RhCoNi NF and next subjected it to solvothermal treatment to undergo a dealloying process with DOT as the etchant of alloy NPs and the ligand for the as-formed MOFs. RhCoNi NFs can release Co^{2+} or Ni^{2+} ions with dissolved oxygen and reacted with linkers to form MOF shell on the alloy NFs. RhCoNi@MOF-74(Ni), pure RhNFs, fcc-Ni, MOF-74(Ni) were measured with hexane and cyclohexene to test the size selectivity effect of RhCoNi@MOF-74(Ni) during the alkene hydrogenation and the results were shown in Fig. 11b: fcc-Ni NPs and pure MOFs all have no catalyst activity; the

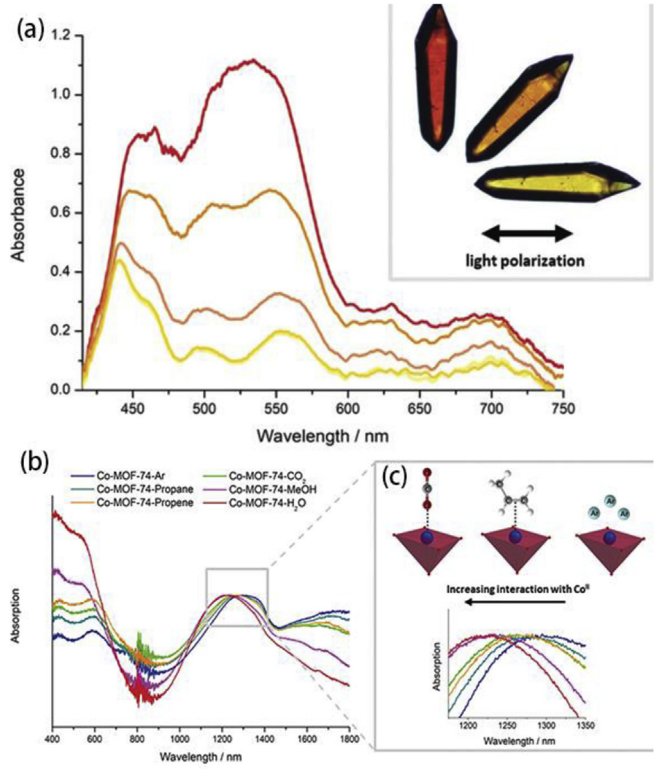

Fig. 7. (a) Spectral of Co-MOF-74 (b) Normalized Vis/NIR-absorption spectra of Co-MOF-74 (c) The maximum position shift of the NIR band [70].

doping of Ni does not significantly affect the catalyst activity comparing with the pure Rh NFs. However, RhCoNi@MOF-74(Ni) perform distinct catalytic performances in the hydrogenation of hexene and cyclohexene. This results shows that MOF-74 as NP@MOF composite shell has great advantages in choosing catalysis. Besides, it is important to clarify the adsorption and mobility of these composites for further study, and related experiments have been reported using MOF-74 supported clusters like Au, Pd, and AuPd [82].

In addition to catalytic selectivity, NP@MOF composite has many notable features. For example, Ni@MOF composites synthesized by the partial thermal decomposition of Ni-MOF-74, shown in Fig. 11 (c), possessed characteristics of porosity and antiferromagnetism just like Ni-MOF-74, as well as the superparamagnetic properties from the isolated Ni NPs [83]. Besides Ni-MOF-74, MOF-74 with other metal ions such as Co, Mn, Fe, Zn, Cu [84] or Mg can also used to synthesize NP/MOF. What's more, metal oxides can also be used to synthesize NP/MOF composite materials with good properties. For example, Fe_3O_4@Mg-MOF-74 core–shell nanoparticles show high efficient capture of glycopeptides [85].

3.4.4. Catalytic activity controlled by charge-transfer interactions

Catalytic performance is influenced by many factors, and recently charge transfer interactions have also been reported as one of them [86]. A charge-transfer interaction between Pt nanoparticles(NPs) and MOFs has been reported, which can control the catalytic activity of Pt NPs supported on MOFs including MOF-74 [87]. The results showed the electronic band energy of the MOF supports apparently affects the activity of the loaded Pt NPs for heterogeneous catalysis due to the charge transfer interaction. From this point of view, the activity of various metal catalysts can be well regulated by choosing appropriate functional groups of central metals, ligands or MOF carriers.

4. Derivative

4.1. MM-MOF-74

By analogy with the synthesis of a multivariate MOF-5 [34], MOF-74 with 2, 4, 6, 8, and 10 different metals have also been reported to be synthesized into mixed metal MOFs (MM-MOFs) [88]. The combination of metal ions for the synthesis of five MM-MOF-74 is shown in Fig. 12 (a). PXRD analysis of MM-MOF-74 series shown in Fig. 12 (b) shows that the crystallinity is consistent with MOF-74 structure, indicating that the topological structure of MM-MOFs doesn't change, and therefore all members are isomorphic.

In addition, another MOF-74 containing two kinds of metal ions Ni and Fe which shows spontaneous magnetization has also been reported. The presence of iron helps to control the doping of isostructural as well as mixed metal solid solutions in one pot synthesis of Ni-MOF-74. NiFe-MOF-74 solids display both porosity and ferrimagnetic ordering compare with the undoped phase because the modulation of spin state in a variable spin inner chain and interchain magnetic interactions [89].

4.2. IRMOF-74

A large aperture is one of the important advantages of MOF-74 because they allow access of molecules for storage, separation, or conversion. Therefore, increasing the pore size of MOF-74 is of great importance to its application. Deng et al. report a strategy to expand the pore aperture of MOF-74 into a previously unattained size regime [90]. The original pore size of MOF-74 are expanded from dioxidoterephthalate link of one phenylene ring to 2 (II), 3 (III), 4 (IV), 5 (V), 6 (VI), 7 (VII),9 (IX), and 11(XI) and therefore get an isoreticular series of MOF-74 structures with the dimension of the pore apertures ranging from 14 to 98 Å which are termed IRMOF-74-I to –XI, shown in Fig. 13.

The products they get have good qualities in various aspects: IRMOF-74-IV to –XI have the largest pore apertures reported to the present for a crystalline material, and IRMOF-74-XI in its guest-free form owns the lowest density for a crystal at room temperature. What's more, all IRMOFs have non-interpenetrating structures and strong architectures, and therefore show permanent porosity and high thermal stability.

Since their first synthesis, IRMOF-74s have received extensive attention and various properties have also been studied. On the adsorption mechanism of IRMOFs, Jawahery et al. report a deformation pattern for IRMOF-74-V when it is induced argon adsorption [91]. And it

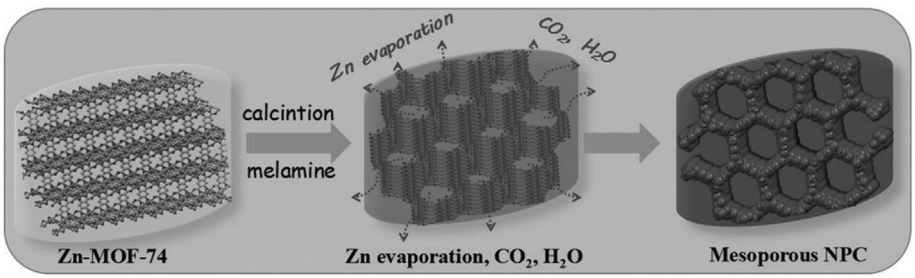

Fig. 8. Preparation for nitrogen doped nanoporous carbon [72].

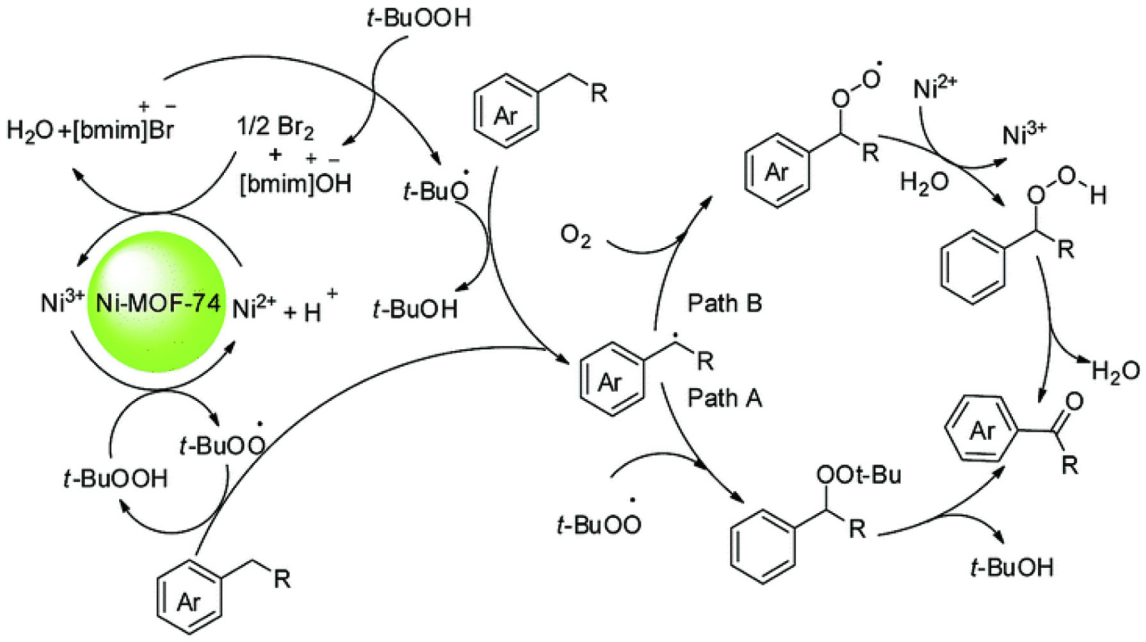

Fig. 9. Oxidation mechanism of benzylic C–H bonds [74].

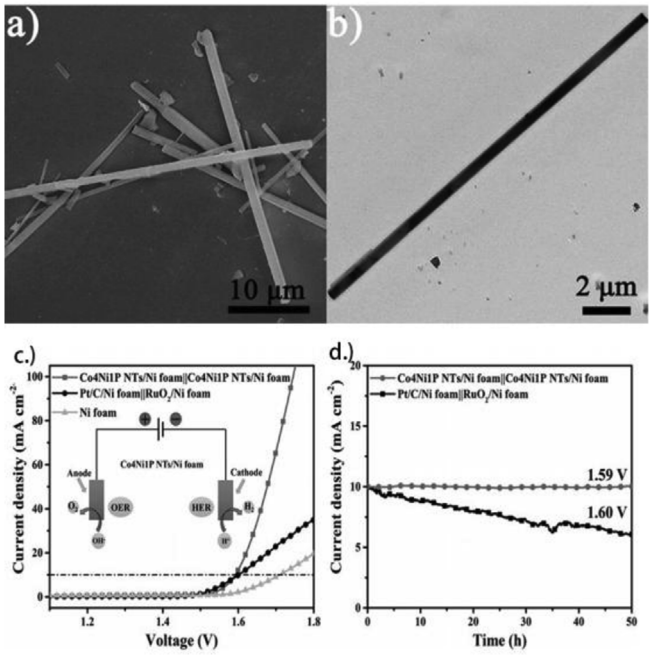

Fig. 10. (a) SEM images and (b) TEM images of MOF-74-$Co_4Ni_1$1 (c) The performance and (d) the catalytic stability of the Co_4Ni_1P NTs and Pt/C-RuO_2 couple for overall water splitting [76].

demonstrates that the deformation IRMOF-74 series undergoes is different from the mechanism of breathing MOFs: neighboring pores in the IRMOF-74 series have different deformation and form repetition in crystalline pattern instead of closing at intermediate pressures and opening at high pressure at the same time like the traditional way. Recently, Liao et al. put forward such a view when studying adsorbate–adsorbate interactions across pore walls in gas adsorption of IRMOF-74: Under the action of pore filling, there can be an interaction between adsorbate and adsorbate, and the adsorbate superlattice can coexist, and the adsorbate superlattice extends beyond the original MOF unit cell [92].

As for their hydrolytic stability, however, experimental results indicate that MOF-74 would be far more stable than IRMOF-1 and IRMOF-10 with respect to water [21]. Besides, isometric network (IR)-MOF-74 extensions have been introduced into molecular gauge building blocks to enable modular assembly of slender and sturdy organic rods with clear and precise lengths ranging from 5 to 50 Å [93].

4.3. M_2(dobpdc)

M_2(dobpdc) (dobpdc^{4-} = 4,4′-dioxido-3,3′-biphenyldicarboxylate) has an expanded MOF-74 structure type. Similar to MOF-74, there are many reports on the synthesis and gas adsorption of this MOF.

For example, M_2(dobpdc) can synthesized very fast even in several minutes using divalent metal oxide colloidal nanocrystals as precursors [94]. For example, ZnO can be used to be synthesized Zn_2(dobpdc) in less than 1 min. And other MOF-74 with different metal ions including Co, Ni, Fe, and Zn can also be successfully synthesized in this way.

In addition, compounds with good carbon dioxide adsorption performance can be obtained through functionalizing coordinatively unsaturated cations with *N*,*N*′-dimethylethylenediamine (mmen). For example, mmen-Mg_2(dobpdc) can be a remarkable new CO_2 adsorbent. The advantage like large capacity, high selectivity, and fast kinetics of adsorbing CO_2 from dry gas mixtures make it great potential in removal CO_2 from air [95]. It is worth mentioning that the coordination of mmen at open metal centers is the key point to explain the unique adsorption mechanism of this compound. Therefore, in order to study the role of the coordination of Mg open metal centers, Xu et al. reported to unravel the local Mg environments in several Mg_2(dobpdc) samples via ^{25}Mg solid-state nuclear magnetic resonance data [96].

4.4. UTSA-74

As an isomer MOF-74, the new metal−organic framework $Zn_2(H_2O)$- (dobdc)·0.5(H_2O) (UTSA-74) showed a high adsorption capacity and separation selectivity for C_2H_2/CO_2. The SOD-type framework structure of UTSA-74 is shown in Fig. 14. It shows UTSA-74 has a secondary building unit by discrete binuclear Zn cluster which is very different from the rod-packing structure of Zn-MOF-74. And the pore channel of UTSA-74 is one-dimensional about 8.0 Å. Besides, UTSA-74 has two kinds of Zn^{2+} atoms: one is tetrahedral and saturated Zn_1, and the other is octahedral Zn_2 having two accessible sites on each metal

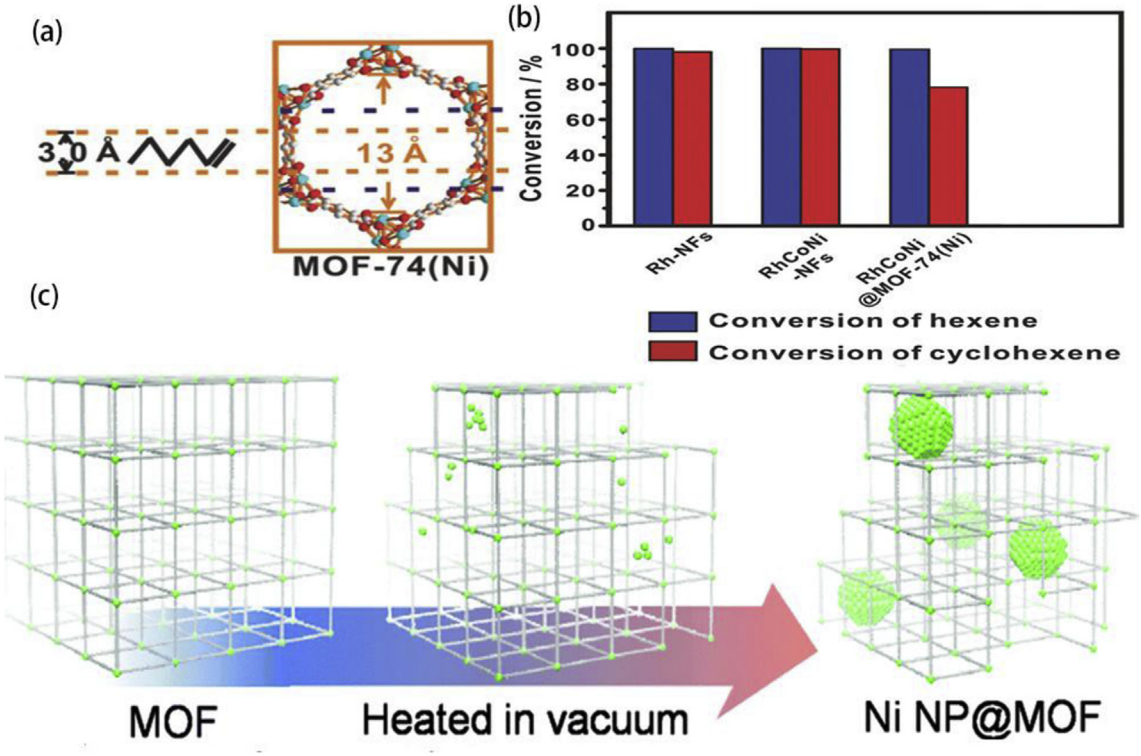

Fig. 11. (a) The molecule sizes of hexane and cyclohexene and the pore size of Ni-MOF-74. (b) The conversion of hydrogenation of hexene and cyclohexene for different catalyst [80]. (c) synthesis of Ni NPs@MOF [83].

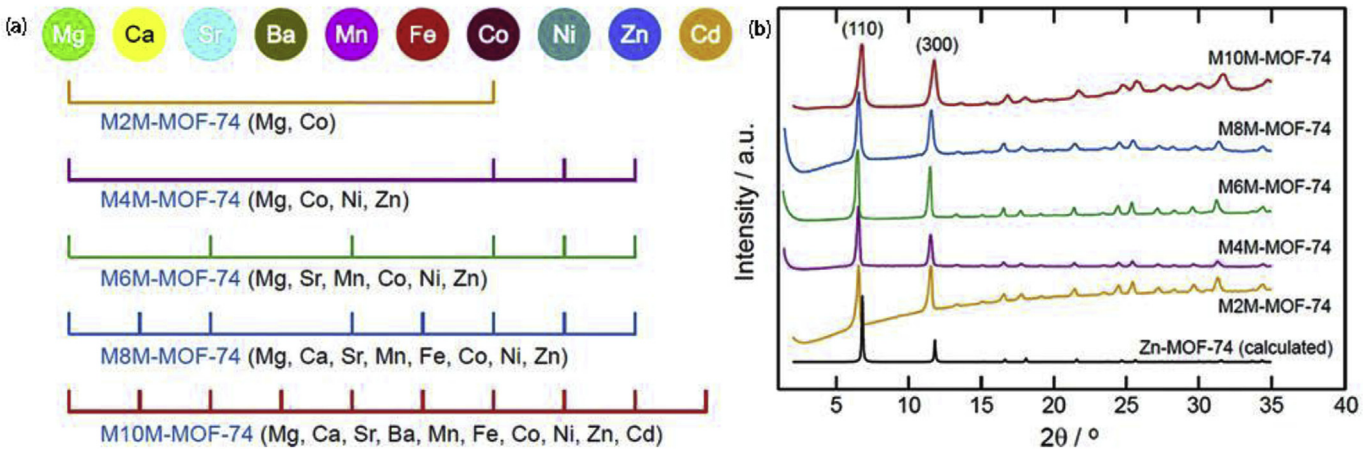

Fig. 12. (a) Synthesis of MM-MOF-74 by metal ion combination method (b) PXRD patterns of MM-MOF-74.

center.

The gas adsorption experiments for MOF-74 and UTSA-74 were conducted together to compare their gas adsorption properties. And the adsorption isotherms of the tested gases were measured from 0 to 100 kPa and the results are shown in Fig. 14g. And it shows that UTSA-74 has an adsorb ability to C_2H_2 comparable to Zn-MOF-74. Meanwhile, its adsorb ability to CO_2 is much lower than Zn-MOF-74. And this adsorption performance illustrates that UTSA-74 is an excellent porous adsorbent which not only has high gas adsorption capacity, but also high gas separation selectivity for the separation of C_2H_2 and CO_2 [97].

4.5. OH-MOF-74

Selective luminescence, a feature of great application value [98], was recently discovered in two novel MOF-74 analogues, and this specific and unique molecular recognition between host porous MOFs and guest molecules makes them great potential in various applications such as luminescent probes for small molecules. Liu et al. reported to synthesize these two MOF-74 analogues (labeled OH-MOF-74) with OH groups (1, OCA-OH and 2, MCA–OH) on 1D channel surfaces through multi-component self-assembly at room temperature [99].

Single-crystal X-ray diffraction analysis reveals both OH-MOF-74 are isomorphous and crystallize in a Rhombohedral space group of R-3. Their guest-free forms demonstrate a potential luminescent probe or sensor for small molecules, and OH-MOF-74 also showed exceptional fluorescence quenching and enhancement behavior for different types of aromatic molecules.

Studies on the solid-state photoluminescence (PL) spectra of 2a (the guest-free form of 2) revealed unique fluorescence quenching and enhancement behavior upon immerging in the solvent of aromatic compounds of group A (having electron-withdrawing groups) and group B (having electron-donating groups) respectively. The results

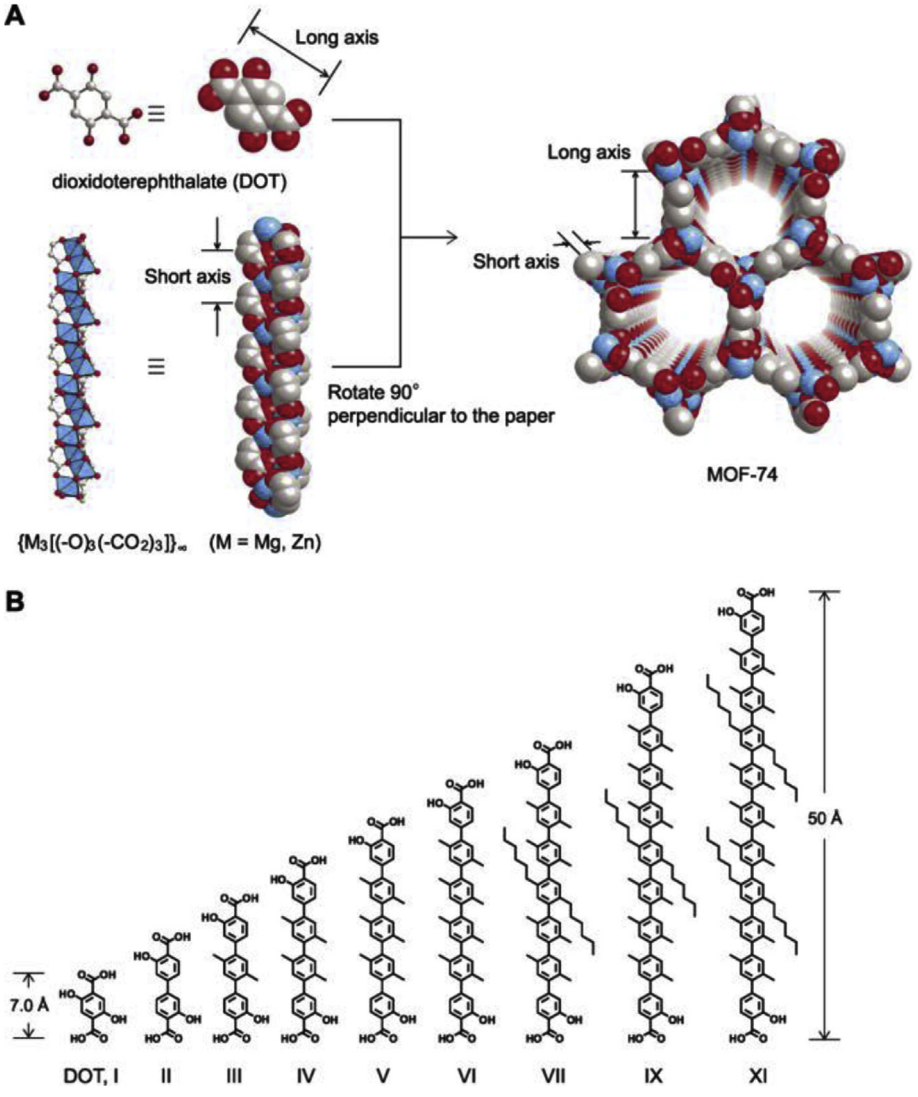

Fig. 13. (A) Crystal structure of MOF-74. (B) Organic links structure used in the synthesis of IRMOFs [90].

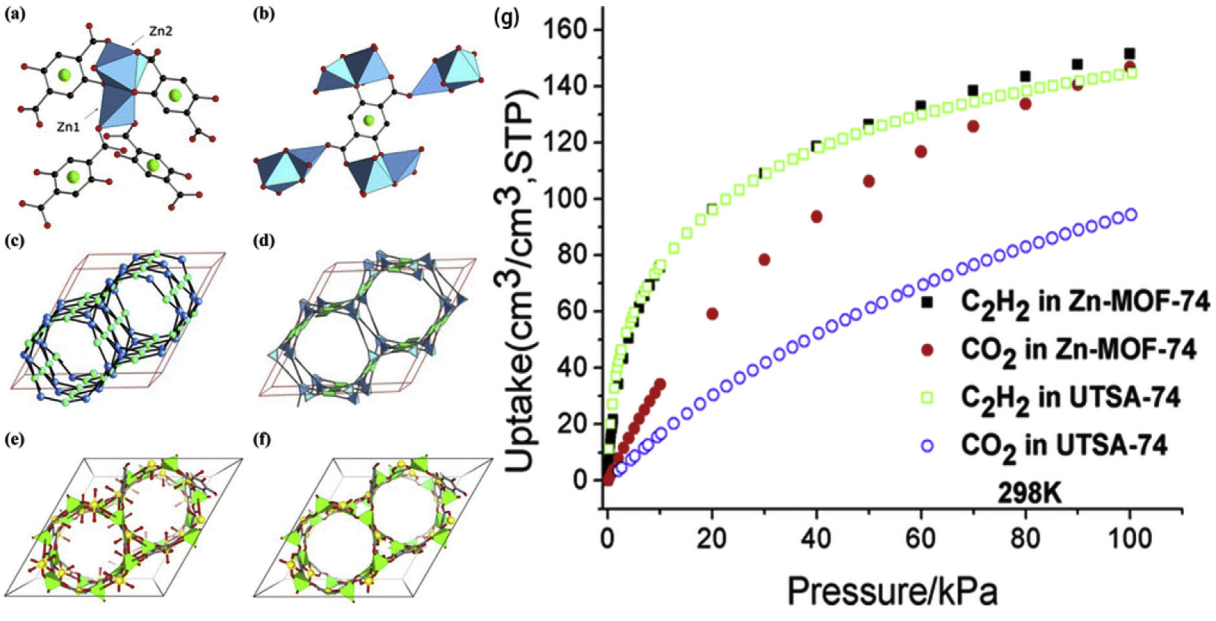

Fig. 14. (a–f) The SOD-type UTSA-74 framework structure (g) Comparison of sorption isotherms for UTSA-74 and Zn-MOF-74 [97].

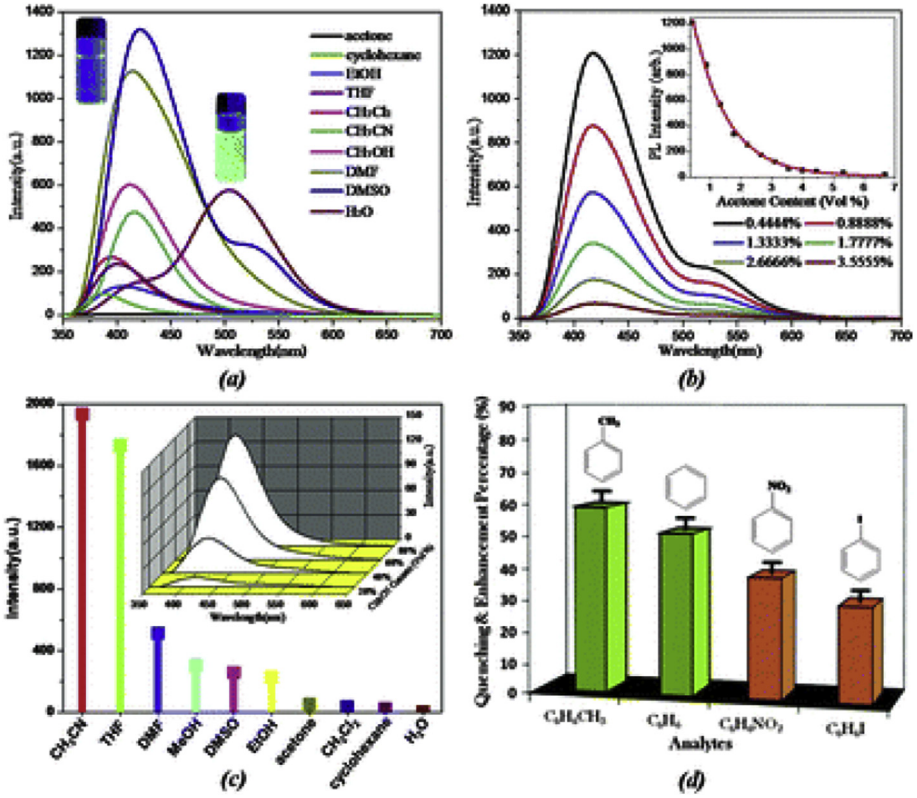

Fig. 15. (a) PL spectra of 1a in different pure solvents. (b) PL spectra of 1a DMSO emulsion. (c) PL intensities of 2a in various pure solvents. (d) Percentage of fluorescence enhancement and quenching of 2a [99].

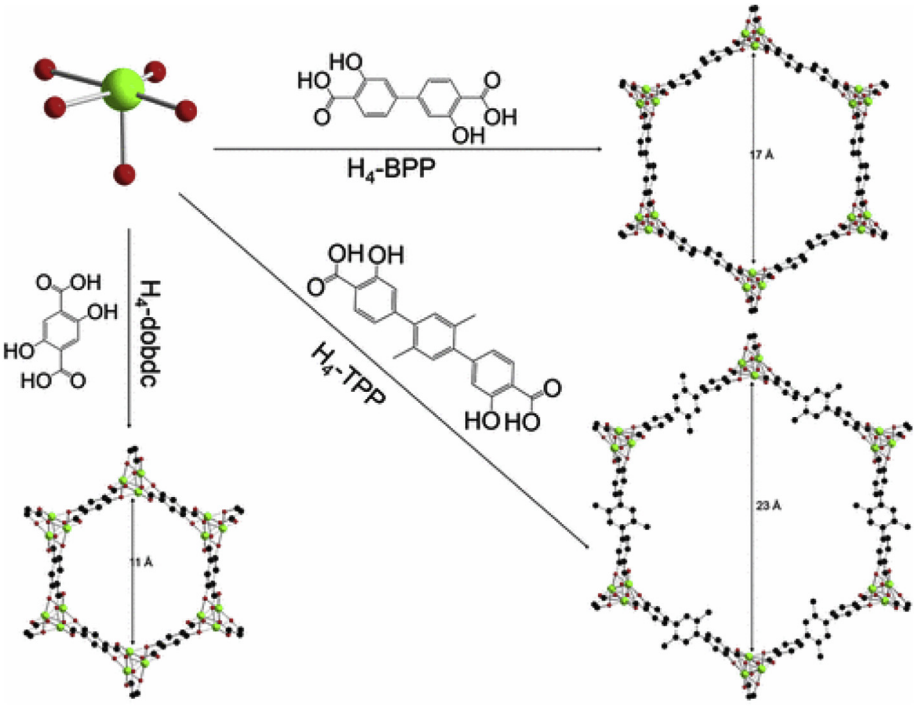

Fig. 16. Sketch Map of the Ni^{2+} node, organic bridging ligands, and the corresponding structures of the pore-expanded Ni-MOF-74 analogues [100].

demonstrate the exceptional ability of 2a to selectively detect different types of aromatic molecules. On the other hand, the PL spectra of 1a and 2a in different solvent emulsions exhibited excellent fluorescence sensing for small molecules. As shown in Fig. 15a and c, the PL intensity was strongly dependent on the solvent molecule. It is assumed that the different binding interactions of the functional OH groups with guest solvent molecules play an important role in such enhancing and quenching effects of small solvent molecules. TGA of all the solvent absorbed forms of the two compounds to demonstrate that the luminescence change of MOF emulsions is solely arisen from the MOF itself

Table 3
The structural characteristics and the performance of adsorbing water and R-134a of Ni-MOF-74 and its derivatives.

	cell volume Å^3	water uptake g g−1	Isotherm of adsorbed water	enthalpies of H_2O adsorption kJ/mol	Uptakes of R134a at P/P_0 = 0.02 g g−1	saturation capacities of R134a g g−1	R-134a isotherms	enthalpies of R-134a adsorption kJ/mol	Ref.
Ni-MOF-74	3323	0.46	type-I	−62.6	0.48	0.58	type-I	−50.6	Zheng et al. [100]
Ni-MOF-74-BPP	9578	0.81	type-I-like	−62.1	0.37	0.75	type-I	−44.2	
Ni-MOF-74-TPP	14680	0.9	type-IV	−60.0	0.28	0.77	type-I	−40.6	

after adsorbing solvents. Different amounts of small solvent molecules absorbed in 1a and 2a shown in the TGA curves reveals the various binding interactions of the functional OH groups with these guest solvent molecules may lead to luminescence change of MOF emulsions. The rational results reveal that 1a and 2a are expected to be used as luminescent probes for detecting small molecules.

4.6. Ni-MOF-74-BPP/-TPP

Three Ni-MOF-74 analogues: Ni-MOF-74, Ni-MOF-74-BPP (BPP = 3,3′-dioxido-4,4′-biphenyldicarboxylate, biphenyl with *para*-COOH), and Ni-MOF-74-TPP (TPP = 3,3′-dioxido-4,4′-triphenyldicarboxylate, triphenyl with *para*-COOH) with excellent adsorption of water and fluorocarbon refrigerant have been reported [100]. The schematic diagram of their structure is shown in Fig. 16. And the related properties of these derivatives are summed up in Table 3.

4.7. CPM

A new CPM family with rod fillers was obtained by simulating the functional group ratio and metal-ligand charge ratio in MOF-74. The syntheses of three members in this CPM family are as follows: CPM-47 can be synthesized by reacting t-BuOLi and H_2obc in a 2:1 M ratio; CPM-48 and CPM-49 can be obtained by using 6-hydroxy-2-naphtholic acid or *trans*-pcoumaric acid as longer bifunctional linkers.

These materials show very high density of guest binding metal sites. Unlike the hetero-helical rod packing in MOF-74, the homo-helical rod-packing in CPM series are not common. The synthesis of this new structure simulating MOF-74 has great significance for constructing materials with high density guest binding metal sites [101].

4.8. M_2(olz)

A new series of expanded analogues of M-MOF-74 was synthesized using the anti-inflammatory drug olsalazine as the sole bridging ligand and named M_2(olz), which showed great potential in drug delivery. M_2(olz) is the first series of bioactive frameworks showing mesoporous porosity, which can be made of various metals. They have 27 Å size pores and the highest Langmuir surface area for MOF with therapeutic connectors. One of the biggest highlights of M_2(olz) frameworks is containing high quantities of the anti-inflammatory olsalazine and releasing them under simulated physiological conditions, leading to intrinsic therapeutic properties. Besides, M_2(olz) can also supply platforms for simultaneous delivery of various therapeutic agents, which have already been demonstrated through the successful encapsulation of phenethylamine in it and release of the two drugs under physiological conditions. The drug-loaded frameworks are shown in Fig. 17 [102].

Besides, there are many reports about MOF-74 analogues. They all show good properties and great prospects in different aspects. For instance: Two new series of isoreticular to MOF-74 termed M-VNU-74-I and -II were synthesized to improve the methanol uptake capacities. They exhibited high porosity and surface areas as well as the highest reported methanol uptake. Therefore, these excellent properties are conducive to their practical application like adsorption heat pump applications and thermal battery systems [103]. And Mn_2(DSBDC), a MOF-74 analogue has great charge mobility, and achieved by replacing phenoxide with thiophenoxide groups [104].

5. Conclusions

In conclusion, we review the latest synthesis methods, properties and applications of MOF-74 as well as its derivatives in recent years.

Some novel synthetic methods have been put forward, such as the template-free synthesis, synthesis from divalent metal oxide colloidal nanocrystals and so on. They not only save time and cost, but also

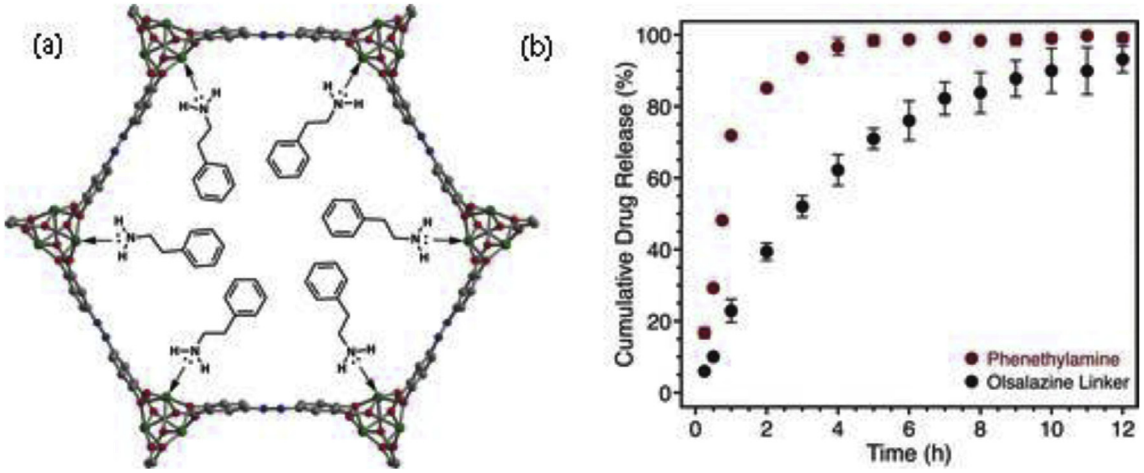

Fig. 17. (a) The reaction of model drug at Mg_2(olz) open metal sites. (b) Release of drug out of Mg_2(olz)$(PEA)_2$ under simulated biological conditions [102].

reduce the pollution to the environment. What's more, the mesopores in MOF-74 can be adjusted to as small as 15 nm stably at room temperature. As for characterization, the results show MOF-74 possesses good hydrolysis stability, highly stable structure, which will be of great significance in its further application.

The biggest highlight of MOF-74 which is also its most widely studied point is its excellent CO_2 adsorption capacity, among which the performance of Mg-MOF-74 is particularly prominent. In addition, we also summarized the performance of MOF-74 in other gases such as hydrogen and oxygen adsorption. Besides, it also has extraordinary performance in gas sensors and it also has extraordinary performance in gas sensors and catalysts, catalysts and many other aspects.

In addition, synthetic materials with excellent properties can be obtained by reasonably combining MOF-74 with other components. Therefore, MOF-74 and its derivatives have great potential and research value in various applications.

We believe with more in-depth research, MOF-74 will have more development and wider application as well as brighter future in our daily life.

Conflicts of interest

The authors declare no conflict of interest.

Acknowledgements

This work was supported by the National Natural Science Foundation of China (Grant No. 51603052) and the Fundamental Research Funds for the Central Universities (Grant No. 18lgpy02).

References

[1] Jian-Rong Li, Ryan J. Kuppler, Hong-Cai Zhou, Selective gas adsorption and separation in metal–organic frameworks, Chem. Soc. Rev. 38 (2009) 1477–1504.
[2] O.K.F. JeongYong Lee, John Roberts, Karl A. Scheidt, SonBinh T. Nguyen, Joseph T. Hupp, Metal–organic framework materials as catalysts, Chem. Soc. Rev. 38 (2009) 1450–1459.
[3] J.E. Nathaniel, L. Rosi, Eddaoudi Mohamed, David T. Vodak, Jaheon Kim, Hydrogen storage in microporous metal-organic frameworks, Science 300 (2003) 1127–1129.
[4] H.S. BoLiu, Hailong Jiang, Xinbo Zhang, Qiang Xu, Metal-organic framework (MOF) as a template for syntheses of nanoporous carbons as electrode materials for supercapacitor, Carbon 48 (2010) 456–463.
[5] K.E.C. Hiroyasu Furukawa, Michael O'Keeffe, Omar M. Yaghi, The chemistry and applications of metal-organic frameworks, Science 341 (2013) 1230444.
[6] a.O.M.Y., Andrew R. Millward, Metal－Organic frameworks with exceptionally high capacity for storage of carbon dioxide at room temperature, J. Am. Chem. Soc. 127 (2005) 17998–9.
[7] a.O.M.Y. Jesse, L.C. Rowsell, Effects of functionalization, catenation, and variation of the metal oxide and organic linking units on the low-pressure hydrogen adsorption properties of Metal－Organic frameworks, J. Am. Chem. Soc. 128 (2006) 1304–1315.
[8] H.F. David Britt, Bo Wang, T. Grant Glover, Omar M. Yaghi, Highly efficient separation of carbon dioxide by a metal-organic framework replete with open metal sites, Proc. Natl. Acad. Sci. Unit. States Am. 106 (2009) 20637–20640.
[9] B.B. Ulrike Böhme, Carolin Paula, Andreas Kuhnt, Wilhelm Schwieger, Alexander Mundstock, Jürgen Caro, Martin Hartmann, Ethene/ethane and propene/propane separation via the olefin and paraffin selective metal–organic framework adsorbents CPO-27 and ZIF-8, Langmuir 29 (2013) 8592–8600.
[10] M.X. Siru Chen, Yanqiang Li, Ying Pan, Liangkui Zhu, Shilun Qiu, Rational design and synthesis of $Ni_xCo_{3-x}O_4$ nanoparticles derived from multivariate MOF-74 for supercapacitors, J. Mater. Chem. 3 (2015) 20145–20152.
[11] M.D.G. Daniel Ruano, Almudena Alfayate, Dr Manuel Sánchez-Sánchez, Nanocrystalline M–MOF-74 as heterogeneous catalysts in the oxidation of cyclohexene: correlation of the activity and redox potential, ChemCatChem 7 (2015) 674–681.
[12] D.F.-J. María, C. Bernini, Marcelo Pasinetti, Antonio J. Ramirez-Pastora, Randall Q. Snurr, Screening of bio-compatible metal–organic frameworks as potential drug carriers using Monte Carlo simulations, J. Mater. Chem. B 2 (2014) 766–774.
[13] J.K. Nathaniel, L. Rosi, Eddaoudi Mohamed, Banglin Chen, Michael O'Keeffe, Omar M. Yaghi, Rod packings and Metal－Organic frameworks constructed from rod-shaped secondary building units, J. Am. Chem. Soc. 127 (2005) 1504–1518.
[14] H.F. David Britt, Bo Wang, T. Grant Glover, Omar M. Yaghi, Chemical filter catches CO_2, PANS (Pest. Artic. News Summ.) 106 (2009) 20551–20552.
[15] P.A. Julien, K. Uzarevic, A.D. Katsenis, S.A. Kimber, T. Wang, O.K. Farha, et al., In situ monitoring and mechanism of the mechanochemical formation of a microporous MOF-74 framework, J. Am. Chem. Soc. 138 (2016) 2929–2932.
[16] Y. Yue, Z.A. Qiao, P.F. Fulvio, A.J. Binder, C. Tian, J. Chen, et al., Template-free synthesis of hierarchical porous metal-organic frameworks, J. Am. Chem. Soc. 135 (2013) 9572–9575.
[17] Manuel Díaz-García, Ivaro Mayoral, Isabel Díaz, M.S.-S. nchez, Nanoscaled M-MOF-74 materials prepared at room temperature, Cryst. Growth Des. 14 (2014) 2479–2487.
[18] J.A.K.W. Wong-Ng, H. Wu, M. Suchomel, Synchrotron X-ray studies of metal-organic framework M_2(2,5-dihydroxyterephthalate), M = (Mn, Co, Ni, Zn) (MOF-74), Powder Diffr. 27 (2012) 256–262.
[19] The 230 Space Groups, International Tables for Crystallography, 2016, pp. 193–687.
[20] S.Z. Kui Tan, Qihan Gong, Pieremanuele Canepa, Hao Wang, Li Jing, Yves J. Chabal, Timo Thonhauser, Water reaction mechanism in metal organic frameworks with coordinatively unsaturated metal ions: MOF-74, Chem. Mater. 26 (2014) 6886–6895.
[21] Sang Soo Han, Seung-Hoon Choi, Adri C.T. van Duin, Molecular dynamics simulations of stability of metal–organic frameworks against H_2O using the ReaxFF reactive force field, Chem. Commun. 46 (2010) 5713–5715.
[22] E.S. Sanil, Kyung-Ho Cho, Do-Young Hong, Ji Sun Lee, Su-Kyung Lee, Sam Gon Ryu, Hae Wan Lee, Jong-San Chang, Young Kyu Hwang, A polyhedral oligomeric silsesquioxane functionalized copper trimesate, Chem. Commun. 51 (2015) 8418–8420.
[23] S.L. Bong Lim Suh, Jihan Kim, Size-matching ligand insertion in MOF-74 for enhanced CO_2 capture under humid conditions, J. Phys. Chem. C 121 (2017) 24444–24451.
[24] M.H. Takashi Kajiwara, Daisuke Watanabe, Hideyuki Higashimura, Teppei Yamada, Hiroshi Kitagawa, A systematic study on the stability of porous coordination polymers against ammonia, Chem. Eur J. 20 (2014) 15611–15617.
[25] J.D.H. Kyuho Lee, Li-Chiang Lin, Berend Smit, Jeffrey B. Neaton, Small-molecule adsorption in open-site Metal－Organic frameworks: a systematic density functional theory study for rational design, Chem. Mater. 27 (2015) 668–678.
[26] G.P. Arpan Kundu, Kaido Sillar, Joachim Sauer, Ab initio prediction of adsorption isotherms for small molecules in Metal－Organic frameworks, J. Am. Chem. Soc.

138 (2016) 14047–14056.
[27] K.S.a.J. Sauer, Ab initio prediction of adsorption isotherms for small molecules in Metal – Organic frameworks: the effect of lateral interactions for methane/CPO-27-Mg, J. Am. Chem. Soc. 134 (2012) 18354–18365.
[28] G.W.P.T. Grant Glover, Bryan J. Schindler, David Britt, Omar Yaghi, MOF-74 building unit has a direct impact on toxic gas adsorption, Chem. Eng. Sci. 66 (2011) 163–170.
[29] D.B. Gerard Alonso, Fatemeh Keshavarz, Xavier Gimenez, Pablo Gamallo, Ramon Sayó s, Density functional theory-based adsorption isotherms for pure and flue gas mixtures on Mg-MOF-74. Application in CO_2 capture swing adsorption processes, J. Phys. Chem. C 122 (2018) 3945–3957.
[30] A.R.M.a.O.M. Yaghi, Metal-organic frameworks with exceptionally high capacity for storage of carbon dioxide at room temperature, J. Am. Chem. Soc. 127 (2005) 17998–17999.
[31] D.T. David Britt, Omar M. Yaghi, Metal-organic frameworks with high capacity and selectivity for harmful gases, 105 (2008) 11623–11627.
[32] L. Zongbi Bao, Qilong Ren, Xiuyang Lu, Shuguang Deng, Adsorption of CO_2 and CH_4 on a magnesium-based metal organic framework, J. Colloid Interface Sci. 353 (2011) 549–556.
[33] Y.W. Jian Liu, Annabelle I. Benin, Paulina Jakubczak, Richard R. Willis, M. Douglas LeVan, CO_2/H_2O adsorption equilibrium and rates on Metal – Organic frameworks: HKUST-1 and Ni/DOBDC, Langmuir 26 (2010) 14301–14307.
[34] H.D. Deng, C. J, H. Furukawa, R.B. Ferreira, J. Towne, C.B. Knobler, B. Wang, O.M. Yaghi, Multiple functional groups of varying ratios in metal-organic frameworks, Science 327 (2010) 846–850.
[35] Antek G. Wong-Foy, Adam J. Matzger, Omar M. Yagh, Exceptional H_2 saturation uptake in microporous Metal – Organic frameworks, J. Am. Chem. Soc. 128 (2006) 3494–3495.
[36] G. Ferey, Hybrid porous solids: past, present, future, Chem. Soc. Rev. 37 (2008) 191–214.
[37] L.J.M. Eric D. Bloch, Wendy L. Queen, Sergey N. Maximoff Sachin Chavan, Julian P. Bigi, Rajamani Krishna, Vanessa K. Peterson, 3 Fernande Grandjean, O. gary J. Long, Berend Smit, Silvia Bordiga, Craig M. Brown, Jeffrey R. Long, selective binding of O_2 over N_2 in a redox-active metal-organic framework with open iron (II) coordination sites, J. Am. Chem. Soc. 133 (2011) 14814–14822.
[38] J.-F.o.V. Nour Nijem, Lingzhu Kong, Haohan Wu, Yonggang Zhao, Li Jing, David C. Langreth, Yves J. Chabal, Molecular hydrogen “pairing” interaction in a metal organic framework system with unsaturated metal centers (MOF-74), J. Am. Chem. Soc. 132 (2010) 14834–14848.
[39] B.B. Stephen A. FitzGerald, Michael Friedman, Jesse B. Hopkins, Christopher J. Pierce, Jennifer M. Schloss, Benjamin Thompson, Jesse L.C. Rowsel, Metal-specific interactions of H_2 adsorbed within isostructural metal-organic frameworks, J. Am. Chem. Soc. 133 (2011) 20310–8.
[40] L.K. Nour Nijem, Yonggang Zhao, Haohan Wu, Li Jing, David C. Langreth, Yves J. Chabal, Spectroscopic evidence for the influence of the benzene sites on tightly bound H_2 in metal organic frameworks with unsaturated metal centers: MOF-74-Cobalt, J. Am. Chem. Soc. 133 (2011) 4782–4784.
[41] Jesse L.C. Rowsell, Omar M. Yaghi, Effects of functionalization, catenation, and variation of the metal oxide and organic linking units on the low-pressure hydrogen adsorption properties of metal-organic frameworks, J. Am. Chem. Soc. 128 (2006) 1304–1315.
[42] R.K.B. Vitalie Stavila, Todd M. Alam, Eric H. Majzoub, Mark D. Allendorf, Reversible hydrogen storage by $NaAlH_4$ confined within a titanium-functionalized MOF-74(Mg) nanoreactor, ACS Nano 6 (2012) 9807–9817.
[43] I.S. Hyunchul Oh, Andreas Mavrandonakis, Thomas heine, Michael Hirscher, highly effective hydrogen isotope separation in nanoporous metal organic frameworks with open metal sites: direct measurement and theoretical analysis, ACS Nano 8 (2014) 761–770.
[44] R.B.-X. Jin Yeong Kim,ˈLinda Zhang, Sung Gu Kang, Michael Hirscher, Hyunchul Oh, Hoi Ri Moon, Exploiting diffusion barrier and chemical affinity of Metal – Organic frameworks for efficient hydrogen isotope separation, J. Am. Chem. Soc. 139 (2017) 15135–15141.
[45] C.J.P. Stephen, A. FitzGerald, Jesse L.C. Rowsell, Eric D. Bloch, Jarad A. Mason, Highly selective quantum sieving of D_2 from H_2 by a Metal – Organic framework as determined by gas manometry and infrared spectroscopy, J. Am. Chem. Soc. 135 (2013) 9458–9464.
[46] H.-Y.C. Da-Ae Yang, Jun Kim, Seung-Tae Yang, Wha-Seung Ahn, CO_2 capture and conversion using Mg-MOF-74 prepared by a sonochemical method, Energy Environ. Sci. 5 (2012) 6465–6473.
[47] S.C. Shyamapada Nandi, Debanjan Chakraborty, Debasis Banerjee, Praveen K. Thallapally, Tom K. Woo, Ramanathan Vaidhyanathan, Ultralow parasitic energy for postcombustion CO_2 capture realized in a nickel isonicotinate Metal – Organic framework with excellent moisture stability, J. Am. Chem. Soc. 139 (2017) 1734–1737.
[48] J.M.L. Huck, L. C, A.H. Berger, M.N. Shahrak, R.L. Martin, A.S. Bhown, M. Haranczyk, K. Reuter, B. Smit, Evaluating different classes of porous materials for carbon capture, Energy Environ. Sci. 7 (2014) 4132.
[49] R.P. Walter, S. Drisdell, Thomas M. McDonald, Jeffrey R. Long, Berend Smit, Jeffrey B. Neaton, David Prendergast, Jeffrey B. Kortright, Probing adsorption interactions in Metal – Organic frameworks using X ray spectroscopy, J. Am. Chem. Soc. 135 (2013) 18183–18190.
[50] E.S. Xueqian Kong, Wen Ding, Jarad A. Mason, Jeffrey R. Long, Jeffrey A. Reimer, CO_2 dynamics in a Metal – Organic framework with open metal sites, J. Am. Chem. Soc. 134 (2012) 14341–14344.
[51] K.S. Jarad, A. Mason, Zoey R. Herm, Rajamani Krishna, Jeffrey R. Long, Evaluating metal–organic frameworks for post-combustion carbon dioxide capture via temperature swing adsorption, Energy Environ. Sci. 4 (2011) 3030–3040.
[52] W.L.H. Queen, M. R. Bloch, E. D, J.A. Mason, M.I. Gonzalez, J.S. Lee, D. Gygi, J.D. Howe, K. Lee, T.A. Darwish, et al., Comprehensive study of carbon dioxide adsorption in the metal-organic frameworks M_2(dobdc) (M = Mg, Mn, Fe, Co, Ni, Cu,Zn), Chem. Sci. 5 (2014) 4569–4581.
[53] R.L. Poloni, K. Berger, R. F, B. Smit, J.B. Neaton, Understanding trends in CO_2 adsorption in metal-organic frameworks with open-metal sites, J. Phys. Chem. Lett. 5 (2014) 861–865.
[54] E.B. Haldoupis, H. J. Shi, K.D. Vogiatzis, P. Bai, W.L. Queen, L. Gagliardi, J.I. Siepmann, Ab initio derived force fields for predicting CO_2 adsorption and accessibility of metal sites in the metal-organic frameworks M-MOF-74 (M = Mn, Co, Ni, Cu), J. Phys. Chem. C 119 (2015) 16058–16071.
[55] J.H. Tim, M. Becker, David Dubbeldam, Li-Chiang Lin, Thijs J.H. Vlugt, Polarizable force fields for CO_2 and CH_4 adsorption in M-MOF-74, J. Phys. Chem. C 121 (2017) 4659–4673.
[56] J.D.H. Robert, M. Marti, Cody R. Morelock, Mark S. Conradi, Krista S. Walton, David S. Sholl, Sophia E. Hayes, CO_2 dynamics in pure and mixed-metal MOFs with open metal sites, J. Phys. Chem. C 121 (2017) 25778–25787.
[57] S.Z. Kui Tan, Qihan Gong, Yuzhi Gao, Nour Nijem, Li Jing, Timo Thonhauser, Yves J. Chabal, Competitive coadsorption of CO_2 with H_2O, NH_3, SO_2, NO, NO_2, N_2, O_2, and CH_4 in M-MOF-74 (M = Mg, Co, Ni): the role of hydrogen bonding, Chem. Mater. 27 (2015) 2203–2217.
[58] S.Z. Kui Tan, Hao Wang, Pieremanuele Canepa, Karim Soliman, Jeremy Cure, Li Jing, Timo Thonhauser, Yves J. Chabal, Interaction of acid gases SO_2 and NO_2 with coordinatively unsaturated metal organic frameworks: M-MOF-74 (M = Zn, Mg, Ni, Co), Chem. Mater. 29 (2017) 4227–4235.
[59] D.G.M. Amrit Kumar, Matteo Lusi, Kai-Jie Chen, Emma A. Daniels, Teresa Curtin, J. John, I.V. Perry, Michael J. Zaworotko, Direct air capture of CO_2 by physisorbent materials, Angew. Chem. Int. Ed. 54 (2015) 14372–14377.
[60] T.-H.B.a.J.R. Long, CO_2/N_2 separations with mixed-matrix membranes containing Mg_2(dobdc) nanocrystals, Energy Environ. Sci. 6 (2013) 3565–3569.
[61] M.M.S. Haiqing Li, Kiyonori Suzuki, Raffaele Ricco, Christian Doblin, Anita J. Hill, Seng Lim, Paolo Falcaro, Matthew R. Hill, Magnetic metal–organic frameworks for effi cient carbon dioxide capture and remote trigger release, Adv. Mater. 28 (2016) 1839–1844.
[62] K.K. Richelle Lyndon, Aaron W. Thornton, Aaron J. Seeber, Bradley P. Ladewig, Matthew R. Hill, Visible light-triggered capture and release of CO_2 from stable metal organic frameworks, Chem. Mater. 27 (2015) 7882–7888.
[63] R.R.C.R.P. Lively, W.J. Koros, Enabling low-cost CO_2 capture via heat integration, Ind. Eng. Chem. Res. 49 (2010) 7550–7562.
[64] S.L. Fateme Rezaei, Hooman Hosseini, Harshul Thakkar, Hajari Amit, Saman Monjezi, Ali A. Rownaghi, MOF-74 and UTSA-16 film growth on monolithic structures and their CO_2 adsorption performance, Chem. Eng. J. 313 (2017) 1346–1353.
[65] W.C.I. Kyuho Lee, Allison L. Dzubak, Pragya Verma, Samuel J. Stoneburner, Li-Chiang Lin, et al., Design of a Metal – Organic framework with enhanced back bonding for separation of N_2 and CH_4, J. Am. Chem. Soc. 136 (2014) 698–704.
[66] L.Z. Yijun Liao, Mitchell H. Weston, William Morris, Joseph T. Huppa, Omar K. Farha, Tuning ethylene gas adsorption via node modulation: Cu-MOF-74 for a high ethylene deliverable capacity, Chem. Commun. 53 (2017) 937 metal 6–9.
[67] B.M. Soumya Mukherjee, Aamod V. Desai, Yuefeng Yin, Rajamani Krishna, Ravichandar Babarao, Sujit K. Ghosh, Harnessing Lewis acidic open metal sites of metal–organic frameworks: the foremost route to achieve highly selective benzene sorption over cyclohexane, Chem. Commun. 52 (2016) 8215–8218.
[68] D.-W.L. WooSeok Jeonga, Sungjune Kimc, Aadesh Haraled, Minyoung Yoonc, Myunghyun Paik Suhe, Jihan Kim, Modeling adsorption properties of structurally deformed metal–organic frameworks using structure–property map, Proc. Natl. Acad. Sci. Unit. States Am. 114 (2017) 7923–7928.
[69] S.F.L.M.G. Campbell, T.M. Swager, M. Dinca, Chemiresistive sensor arrays from conductive 2D metal-organic frameworks, J. Am. Chem. Soc. 137 (2015) 13780–13783.
[70] A.M. Ina Strauss, Dominik Hinrichs, Rasmus Himstedt, Knebel Alexander, Reinhardt Carsten, Dirk Dorfs, Jrgen, Caro the interaction of guest molecules with Co-MOF-74: a vis/NIR and Raman approach, Angew. Chem. Int. Ed. 57 (2018) 1–6.
[71] S.C.I. Katsounaros, A.R. Zeradjanin, K.J. Mayrhofer, Oxygen electrochemistry as a cornerstone for sustainable energy conversion, Angew. Chem. Int. Ed. 53 (2014) 102.
[72] L.Y.G.C.Z. Wen, Zn-MOF-74 derived N-doped mesoporous carbon as pH-universal electrocatalyst for oxygen reduction reaction, Adv. Funct. Mater. 27 (2017) 1606190.
[73] A.M.P.M. Kai Xu, Binh Khanh Mai, Hajime Hirao, How does CO_2 react with styrene oxide in Co-MOF-74 and Mg-MOF74? Catalytic mechanisms proposed by QM/MM calculations, J. Phys. Chem. C 122 (2018) 503–514.
[74] Y.Z. Changyan Guo, Yi Zhang, Jide Wang, An efficient approach for enhancing the catalytic activity of Ni-MOF-74 via a relay catalyst system for the selective oxidation of benzylic C–H bonds under mild conditions, Chem. Commun. 54 (2015) 3701–3704.
[75] C.K.B. Anthony, F. Cozzolino, Ryan D. Palmer, Junko Yano, Minyuan Li, Ligand redox non-innocence in the stoichiometric oxidation of Mn_2(2,5-dioxidoterephthalate) (Mn-MOF-74), J. Am. Chem. Soc. 136 (2014) 3334–3337.
[76] L.C. Liting Yan, Pengcheng Dai, Xin Gu, Dandan Liu, Liangjun Li, Ying Wang, Xuebo Zhao, Metal-organic frameworks derived nanotube of nickel–cobalt bimetal phosphides as highly efficient electrocatalysts for overall water splitting, Adv. Funct. Mater. 27 (2017) 1703455.
[77] Z.G. Doufeng Wu, Xinbo Yin, Qingqing Pang, Binbin Tu, Lijuan Zhang, Yong-

Gang Wang, Qiaowei Li, Metal–organic frameworks as cathode materials for Li–O_2 batteries, Adv. Mater. 26 (2014) 3258–3262.
[78] L.Z. Chong Qu, Wei Meng, Zibin Liang, Bingjun Zhu, Dai Dang, Shuge Dai, Bote Zhao, Hassina Tabassum, Song Gao, Hao Zhang, Wenhan Guo, Ruo Zhao, Xinyu Huang, Meilin Liu, Ruqiang Zou, MOF-derived a-NiS nanorods on graphene as an electrode for high-energy-density supercapacitors, J. Mater. Chem. 6 (2018) 4003–4012.
[79] W.R.L. Won Ju Phang, Kicheon Yoo, Dae Won Ryu, BongSoo Kim, Chang Seop Hong, pH-dependent proton conducting behavior in a metal–organic framework material, Angew. Chem. Int. Ed. 53 (2014) 8383–8387.
[80] H.-Q.L. Lu-Ning Chen, Meng-Wen Yan, Chao-Fan Yuan, Wen-Wen Zhan, Ya-Qi Jiang, Zhao-Xiong Xie, Qin Kuang, Lan-Sun Zheng, Ternary alloys encapsulated within different MOFs via a self-sacrificing template process: a potential platform for the investig ation of size-selective catalytic performances, Small 13 (2017) 1700683.
[81] T.Y. Kazuki Nakatsuka, Yasutaka Kuwahara, Kohsuke Mori, Hiromi Yamashita, Controlled pyrolysis of Ni-MOF-74 as a promising precursor for the creation of highly active Ni nanocatalysts in size-selective hydrogenation, Chem. Eur J. 24 (2018) 898–905.
[82] K.S.W. Lasse, B. Vilhelmsen, David S. Sholl, Structure and mobility of metal clusters in MOFs: Au, Pd, and AuPd clusters in MOF-74, J. Am. Chem. Soc. 134 (2012) 12807–12816.
[83] H.K. Megumi Mukoyoshi, Kohei Kusada, ab Mikihiro Hayashi, Teppei Yamada, Mitsuhiko Maesato, M. Jared, Taylor, Yoshiki Kubota, Kenichi Kato, Masaki Takata, Tomokazu Yamamoto, Syo Matsumurab, Hiroshi Kitagawa, Hybrid materials of Ni NP@MOF prepared by a simple synthetic method, Chem. Commun. 51 (2015) 12463–12466.
[84] A.L. Ignacio Luz, Daniel T. Sun, Wendy L. Queen, Raffaella Buonsanti, Understanding the formation mechanism of metal Nanocrystal@MOF-74 hybrids, Chem. Mater. 28 (2016) 3839–3849.
[85] J.W. Jie Li, Yun Ling, Zhenxia Chen, Mingxia Gao, Xiangmin Zhang, Yaming Zhou, Unprecedented highly efficient capture of glycopeptides by Fe_3O_4@Mg-MOF-74 core–shell nanoparticles, Chem. Commun. 53 (2017) 4018–4021.
[86] J.A.R.A. Bruix, P.J. Ramirez, S.D. Senanayake, J. Evans, J.B. Park, D. Stacchiola, P. Liu, J. Hrbek, F. Illas, A new type of strong metal-support interaction and the production of H_2 through the transformation of water on Pt/CeO_2(111) and Pt/CeOx/TiO_2(110) catalysts, J. Am. Chem. Soc. 134 (2012) 8968–8974.
[87] M.S. Shotaro Yoshimaru, Aleksandar Staykov, Kenichi Katoc, Miho Yamauchi, Modulation of the catalytic activity of Pt nanoparticles through charge-transfer interactions with metal–organic frameworks, Chem. Commun. 53 (2017) 6720–6723.
[88] H.D. Lisa, J. Wang, Hiroyasu Furukawa, Felipe Gandara, Kyle E. Cordova, Dani Peri, Omar M. Yaghi, Synthesis and characterization of Metal − Organic framework-74 containing 2, 4, 6, 8, and 10 different metals, Inorg. Chem. 53 (2014) 5881–5883.
[89] J.C.W. Víctor Rubio-Gimenez, Juan M. Clemente-Juan, Carlos Martí-Gastaldo, Spontaneous magnetization in heterometallic NiFe-MOF-74 microporous magnets by controlled iron doping, Chem. Mater. 29 (2017) 6181–6185.
[90] S.G. Hexiang Deng, Kyle E. Cordova, Cory Valente, Hiroyasu Furukawa, Mohamad Hmadeh, Felipe Gándara, Adam C. Whalley, Zheng Liu, Shunsuke Asahina, Hiroyoshi Kazumori, Michael O'Keeffe, 1 Osamu Terasaki, J. Fraser Stoddart, Omar M. Yaghi, Large-pore apertures in a series of metal-organic frameworks, Science 336 (2012) 1018–1023.
[91] C.M.S. Sudi Jawahery, Efrem Braun, Matthew Witman, Davide Tiana, Bess Vlaisavljevich, Berend Smit, Adsorbate-induced lattice deformation in IRMOF-74 series, Nat. Commun. 8 (2017) 13945.
[92] H.D. Hae Sung Cho, Keiichi Miyasaka, Zhiyue Dong, Minhyung Cho, Alexander V. Neimark, Jeung Ku Kang, Omar M. Yaghi, Osamu Terasaki, Extra adsorption and adsorbate superlattice formation in metal-organic frameworks, Nature 527 (2015) 503.
[93] C.V. Sergio Grunder, Adam C. Whalley, Srinivasan Sampath, Jrg Portmann, Youssry Y. Botros, J. Fraser Stoddart, Molecular gauge blocks for building on the nanoscale, Chem. Eur J. 18 (2012) 15632–15649.
[94] L. Maserati, S.M. Meckler, C. Li, B.A. Helms, Minute-MOFs: ultrafast synthesis of M_2(dobpdc) metal–organic frameworks from divalent metal oxide colloidal nanocrystals, Chem. Mater. 28 (2016) 1581–1588.
[95] W.R.L. Thomas, M. McDonald, Jarad A. Mason, Brian M. Wiers, Chang Seop Hong, Jeffrey R. Long, Capture of carbon dioxide from air and flue gas in the AlkylamineAppended Metal − Organic framework mmen-Mg_2(dobpdc), J. Am. Chem. Soc. 134 (2012) 7056–7065.
[96] E.S.M.B. Jun Xu, Andrew S. Lipton, Thomas M. McDonald, Yifei Michelle Liu, Berend Smit, Jeffrey R. Long, P. Arno, M. Kentgens, Jeffrey A. Reimer, Uncovering the local magnesium environment in the Metal − Organic framework Mg_2(dobpdc) using 25Mg NMR spectroscopy, J. Phys. Chem. C 121 (2017) 19938–19945.
[97] F. Luo, C. Yan, L. Dang, R. Krishna, W. Zhou, H. Wu, et al., UTSA-74: a MOF-74 isomer with two accessible binding sites per metal center for highly selective gas separation, J. Am. Chem. Soc. 138 (2016) 5678–5684.
[98] C.A.B.M.D. Allendorf, R.K. Bhakta, R.J.T. Houk, Luminescent metal–organic frameworks, Chem. Soc. Rev. 38 (2009) 1330–1352.
[99] Y.-j.Q. Gui-lei Liu, Lei Jing, Gui-yuan Wei, Hui Li, Two novel MOF-74 analogs exhibiting unique luminescent selectivity, Chem. Commun. 49 (2013) 1699.
[100] R.S.V. Jian Zheng, Luis Estevez, Phillip K. Koech, Tamas Varga, Donald M. Camaioni, Thomas A. Blake, B. Peter McGrail, Radha Kishan Motkuri, Pore-engineered Metal − Organic frameworks with excellent adsorption of water and fluorocarbon refrigerant for cooling applications, J. Am. Chem. Soc. 139 (2017) 10601–10604 139(2017) 10601 − 4.
[101] M.S.S. Xiang Zhao, Xitong chen, Xianhui Bu, Pingyun Feng, Homo-helical rod packing as a path toward the highest density of guest-binding metal sites in metal–organic frameworks, Angew. Chem. Int. Ed. 57 (2018) 6208–6211.
[102] T.R. Dana, J. Levine, Matthew T. Kapelewski, Benjamin K. Keitz, Julia Oktawiec, Douglas A. Reed, Jarad A. Mason, Henry Z.H. Jiang, Kristen A. Colwell, Christina M. Legendre, Stephen A. FitzGerald, Jeffrey R. Long, Olsalazine-based Metal − Organic frameworks as biocompatible platforms for H_2 adsorption and drug delivery, J. Am. Chem. Soc. 138 (2016) 10143–10150.
[103] H.L.N. Binh, T. Nguyen, Tranh C. Nguyen, Kyle E. Cordova, Hiroyasu Furukawa, High methanol uptake capacity in two new series of Metal − Organic frameworks: promising materials for adsorption-driven heat pump applications, Chem. Mater. 28 (2016) 6243–6249.
[104] C.H.H. Lei Sun, Mikael A. Minier, Aron Walsh, Mircea Dinca, Million-fold electrical conductivity enhancement in Fe_2(DEBDC) versus Mn_2(DEBDC) (E = S, O), J. Am. Chem. Soc. 137 (2015) 6164–6167.